Atmos. Chem. Phys. Discuss., https://doi.org/10.5194/acp-2018-1026
Manuscript under review for journal Atmos. Chem. Phys.
Discussion started: 30 October 2018

Atmospheric Chemistry and Physics Discussions

Characterising the Seasonal and Geographical Variability of Tropospheric Ozone, Stratospheric Influence and Recent Changes

Ryan S. Williams[1], Michaela I. Hegglin[1], Brian J. Kerridge[2], Patrick Jöckel[3], Barry G. Latter[2] and David A. Plummer[4]

[1] *University of Reading, Reading, UK*
[2] *Rutherford Appleton Laboratory (RAL), Harwell Oxford, Didcot, UK*
[3] *German Aerospace Center (DLR), Institute of Atmospheric Physics, Oberpfaffenhofen-Wessling, Germany*
[4] *Canadian Centre for Climate Modelling and Analysis, Environment and Climate Change Canada, Montréal, QC, Canada*

Correspondence to: Ryan S. Williams (r.s.williams@pgr.reading.ac.uk)

Abstract. The stratospheric contribution to tropospheric ozone (O_3) has been a subject of much debate in recent decades, but is known to have an important influence. Recent improvements in diagnostic and modelling tools provide new evidence that the stratosphere has a much larger influence than previously thought. This study aims to characterise the seasonal and geographical distribution of tropospheric ozone, its variability and changes, and provide quantification of the stratospheric influence on these measures. To this end, we evaluate hindcast specified dynamics chemistry-climate model (CCM) simulations from the ECHAM/MESSy Atmospheric Chemistry (EMAC) model and the Canadian Middle Atmosphere Model (CMAM), as contributed to the IGAC/SPARC Chemistry Climate Model Initiative (CCMI) activity, together with satellite observations from the Ozone Monitoring Instrument (OMI) and ozonesonde profile measurements from the World Ozone and Ultraviolet Radiation Data Centre (WOUDC) over a period of concurrent data availability (2005-2010). An overall positive, seasonally dependent bias in 1000-450 hPa (~ 0-5.5 km) subcolumn ozone is found for EMAC, ranging from 2-8 Dobson Units (DU), whereas CMAM is found to be in closer agreement with the observations, although with substantial seasonal and regional variation in the sign and magnitude of the bias (~ -4 to +4 DU). Although the application of OMI averaging kernels (AKs) improves agreement with model estimates from both EMAC and CMAM as expected, comparisons with ozonesondes indicate a positive ozone bias in the lower stratosphere in CMAM, together with an underestimation of photochemical ozone production (negative bias) in the troposphere. Model variability is found to be more similar in magnitude to that implied from ozonesondes, in comparison with OMI which has significantly larger variability. Noting the overall consistency of the CCMs, the influence of the model chemistry schemes and internal dynamics is discussed in relation to the inter-model differences found. In particular, it is shown that CMAM simulates a faster and shallower Brewer-Dobson Circulation (BDC) relative to both EMAC and observational estimates, which has implications for the distribution and magnitude of the downward flux of stratospheric ozone, over the most recent climatological period (1980-2010). Nonetheless, it is shown that the stratospheric influence on tropospheric ozone is larger than previously thought and is estimated to exceed 50 % in the wintertime extratropics, even in the lower troposphere. Finally, long term changes in the CCM ozone tracers are calculated for different seasons between 1980-89 and 2001-10. An overall statistically significant increase in tropospheric ozone is found across much of the world,

but particularly in the Northern Hemisphere and in the middle to upper troposphere, where the increase is on the order of 4-6 ppbv (5-10 %). Our model study implies that attribution from stratosphere-troposphere exchange (STE) to such ozone changes ranges from 25-30 % at the surface to as much as 50-80 % in the upper troposphere-lower stratosphere (UTLS) across many regions of the world. These findings highlight the importance of a well-resolved stratosphere in simulations of tropospheric ozone and its implications for the radiative forcing, air quality and oxidation capacity of the troposphere.

Key Words: Tropospheric ozone, stratosphere-troposphere exchange (STE), chemistry climate models (CCMs), ozone monitoring instrument (OMI), ozone variability and changes.

1 Introduction

Tropospheric ozone (O_3) has wide ranging implications for air quality, radiative forcing and the oxidation capacity of the troposphere (Fiore et al., 2012; Myhre et al., 2013). Whilst ozone is typically regarded as a pollutant at ground level, adversely affecting human health and ecosystems (Paoletti et al., 2014), it is a primary source of the hydroxyl (OH) radical which acts to cleanse the troposphere by breaking down a number of pollutants, along with some greenhouse gases (Seinfeld and Pandis, 2006; Cooper et al., 2010). Despite this, ozone is also a greenhouse gas itself, exerting the largest radiative forcing in the upper troposphere due to the characteristic low temperatures in the upper troposphere (Lacis et al., 1990). Since ozone has a relatively short global mean lifetime in the troposphere (~ 3 weeks), along with spatially and temporally highly varying sources and sinks (Lelieveld et al., 2009), it is not well mixed and large spatial and temporal variations in ozone abundance thus occur over seasonal, interannual and decadal timescales. This is reinforced by the strong dependence on sunlight as well as precursor emissions, which have both natural and anthropogenic sources (Cooper et al., 2014).

A large fraction of the ozone in the troposphere is formed through photochemical reactions of precursor molecules such as carbon monoxide (CO), nitrogen oxides (NO_x) and volatile organic compounds (VOCs), which have both natural and anthropogenic emission sources. Since the late 19th century however, changes in the tropospheric ozone burden can be largely attributed to anthropogenic precursor emissions, which have led to a significant increase in background ozone concentrations, particularly in the Northern Hemisphere mid-latitudes (Cooper et al., 2010, 2014; Stevenson et al., 2013). Ozone may be produced either in situ or non-local to precursor source regions, as determined by the synoptic meteorology, with the potential for long distance advection prior to photochemical destruction or deposition, given a lifetime of several weeks in the troposphere (Lelieveld et al., 2009). For instance, tropospheric ozone levels across western North America are particularly susceptible to increasing Asian emissions due to long range transport across the Pacific (Hudman et al., 2004; Cooper et al., 2010; Lin et al., 2014, 2015). An additional influence is that of exchange of stratospheric and tropospheric air masses, which leads to a net downward flux of ozone and a subsequent enhanced tropospheric ozone burden (Holton and Lelieveld, 1996; Lamarque et al., 1999), especially in mid-latitude regions (Miles et al., 2015).

Atmos. Chem. Phys. Discuss., https://doi.org/10.5194/acp-2018-1026
Manuscript under review for journal Atmos. Chem. Phys.
Discussion started: 30 October 2018

Stratosphere-troposphere exchange (STE) of air is governed non-locally by the wave-driven large-scale meridional circulation, the Brewer-Dobson Circulation (BDC) (Holton et al., 1995; Shepherd, 2007; Butchart, 2014). The BDC induces preferential troposphere-to-stratosphere transport (TST) in the tropics, in contrast to mid to high latitude regions where stratosphere-to-troposphere transport (STT) must prevail to conserve mass continuity (Holton et al., 1995). The BDC, and thus STE, exhibits strong seasonality in both hemispheres with the circulation strongest during wintertime, but especially in the northern Hemisphere, due to the largest wave-induced forces occurring at this time (Holton et al., 1995). Given a photochemical lifetime of several months in the lower stratosphere, analogous to transport timescales, seasonality in the BDC results in a significant enrichment of ozone and other chemical tracers in the extratropical lower stratosphere over winter (Hegglin et al., 2006; Krebsbach et al., 2006); with the largest mixing ratios achieved close to the tropopause in early summer (Prather et al., 2011; Škerlak et al., 2014). Whilst it is recognised that the cross-tropopause downward flux of ozone in the extratropics reaches a seasonal maximum in late spring and early summer, this incidentally coincides with the downward STE mass flux being close to a seasonal minimum (Škerlak et al., 2014; Yang et al., 2016). This strongly implies that the ozone concentration at the tropopause controls the seasonality in the downward ozone flux. Staley (1962) was the first to note that it is in fact the displacement of the tropopause altitude seasonally in each hemisphere that primarily governs the downward mass flux; maximum in spring as the tropopause rises and minimum in autumn as the tropopause falls relative to the background state. Analysis of deep STE events, where direct entrainment of stratospheric air into the planetary boundary layer (PBL) occurs indicates that the downward transport of ozone is primarily controlled by the mass flux for these events, with a peak in early spring (Škerlak et al., 2014).

Whilst it is accepted that STE is an important and significant source of upper tropospheric ozone (e.g. Holton et al., 1995), the influence on near-surface ozone levels is poorly understood. Globally, Lamarque et al. (1999) estimated that STE increases the average tropospheric column amount by only a modest ~ 11.5 % using a three-dimensional global chemistry transport model. However on a monthly resolved basis, this influence was shown to increase to ~ 10-20 % in the lower troposphere and ~ 40-50 % in the upper troposphere. Furthermore, a number of mid-latitude case studies have demonstrated that STT events may provide a much larger contribution to surface ozone in some seasons (typically spring) and more locally on timescales of hours to days given favourable meteorological conditions. Over a three month period between April and June 2010, Lin et al. (2012) concluded that the stratosphere was the source of 20-30 % of surface O_3 across the western US using the high resolution (~ 50 x 50 km^2) GFDL AM3 chemistry climate model, with episodic enhancements of some 20-40 ppbv of the surface maximum 8-hour average (MD8A) ozone estimated from 13 identified stratospheric intrusion events. Similarly, model-based studies find evidence for a significant stratospheric contribution to the pronounced tropospheric summertime ozone maximum over the eastern Mediterranean and the Middle East (EMME) (Zanis et al., 2014; Akritidis et al., 2016) and the Persian Gulf (Lelieveld et al., 2009), with influence as far down as the PBL where near-surface ozone levels are known to frequently exceed EU air quality standards. In contrast using ozonesonde observations, Greenslade et al. (2017) found only a small stratospheric

contribution (1-3.5 %) to the mean tropospheric ozone burden for three sites neighbouring the Southern Ocean, although with exceedances of 10 % during individual events.

Current understanding of the seasonal and regional climatology of tropospheric ozone is severely constrained by the paucity of in situ measurements from ozonesondes and aircraft measurements, which are spatially and temporally biased, although the advent of satellite remote sensing platforms in recent years for inference of global tropospheric ozone abundance has reduced uncertainty to some extent (Parrish et al., 2014). However, there are inherent limitations with retrieving tropospheric ozone from spaceborne instruments and this has implications for the accuracy of resultant satellite-based climatologies. Although the validation of such satellite data with any limited in situ data available increases confidence in our estimates of the climatology and short term trends, scientists must instead rely on tools such as chemistry climate models (CCMs) to fill in the gaps in our understanding of the global distribution of tropospheric ozone, as well as longer term changes (Cooper et al., 2014). Additionally, CCMs can be used to assess and quantify the causes of tropospheric ozone features through analysis of photochemical production and loss rates, together with transport tracer simulations. The latter can serve to identify the relative importance of in situ photochemical production, long range transport and stratospheric influence. Nonetheless, such simulations are subject to a number of constraints, including limitations in model horizontal and vertical resolution, complexity of the implemented chemistry scheme and the realism of simulated transport characteristics. Above all however, the largest uncertainty by far is the accuracy of the precursor emission inventories used in CCM simulations.

In this study, the seasonal climatology, inter-annual variability and long term evolution of the influence of stratospheric ozone on tropospheric ozone and its geographical dependencies is investigated with the aim to update and extend the findings of Lamarque et al. (1999). A summary of the different data sources used is given in section 2. As a first step in section 3, we test the realism of two state-of-the-art CCMs by comparing their ozone estimates with the ozone distributions derived from the Ozone Monitoring Instrument (OMI) satellite measurements over a common baseline period, together with spatially and temporally limited vertical profile information provided by ozonesondes. Noting the model biases with respect to the observations, the fine scale vertical resolution offered by the CCMs is then exploited to analyse regional and seasonal variations in the vertical distribution of O_3 in section 4, together with ozone of stratospheric origin (O_3S) and the relative contribution of O_3S to O_3 (O_3F) to infer the importance of the stratosphere in determining tropospheric ozone levels. Finally, height resolved seasonal changes in model O_3 and O_3S are examined globally between 1980-1989 and 2001-2010 in section 5. The findings presented in both sections 3 and 4 are also discussed here within the context of the wider literature. Finally, section 6 will provide a summary of the findings, along with an overview of the utility of the models for improving our understanding of the spatial distribution and changes in tropospheric ozone.

Atmos. Chem. Phys. Discuss., https://doi.org/10.5194/acp-2018-1026
Manuscript under review for journal Atmos. Chem. Phys.
Discussion started: 30 October 2018

2. Data Sources

2.1 Chemistry Climate Model (CCM) Simulations

This study uses RefC1SD specified dynamics (SD) hindcast simulations, conducted for the Chemistry Climate Model Initiative (CCMI-1) (Morgenstern et al., 2017), of both ozone (O_3) and stratosphere-tagged tracer ozone (O_3S) for the period 1980-2010 inclusive from two state-of-the-art CCMs (Hegglin and Lamarque, 2015). For each simulation, prognostic variables (temperature, vorticity, divergence, and surface pressure) from the ERA-Interim reanalysis dataset are used to nudge the CCM towards the observed atmospheric state through Newtonian relaxation, with corresponding relaxation times of 24, 6, 48 and 24 h respectively for EMAC (Jöckel et al., 2016) and 24 h for all four variables in CMAM (McLandress et al., 2013). Variability in sea surface temperatures (SSTs) and sea ice concentration directly accounted for from ERA-Interim in the case of EMAC, but is instead derived from the HadISST dataset provided from the UK Met Office Hadley Centre for CMAM (Morgenstern et al., 2017; Rayner et al., 2003). Furthermore, each model includes prescribed decadal emissions of anthropogenic and natural greenhouse gas (GHG) and ozone precursor emissions (which act as a forcing) from the Coupled Model Intercomparison Phase 5 (CMIP5) database, alongside variability induced by other natural forcings such as solar activity and volcanic eruptions in most simulations (Brinkop et al., 2016). All simulations used are compliant with the Chemistry-Climate Model Initiative (CCMI) definitions specified by the IGAC and SPARC communities (Eyring et al., 2013). For full details of the model chemistry treatments and emission inventories used, the reader is directed to the CCMI review paper by Morgenstern et al. (2017), as well as Jöckel et al. (2016) for EMAC and the relevant section of Pendlebury et al. (2015) for CMAM. Only the main differences between the two models are briefly summarised here.

2.1.1 EMAC

RC1SD-base-10 simulations (without nudging of the global mean temperature) from the interactively coupled European Centre for Medium-Range Weather Forecasts – Hamburg (ECHAM)/Modular Earth Submodel System (MESSy) Atmospheric Chemistry (EMAC) model are used in this study, which have a T42 (triangular) spectral resolution, equating to a Quadratic Gaussian grid of ~ 2.8° by 2.8°, and 90 vertical hybrid sigma pressure levels up to 0.01 hPa (Jöckel et al., 2016). EMAC uses the flux-form semi Langrangian transport (FFST) scheme for chemical and meteorologically active constituents, physical tracers, water vapour, as well as other chemical tracers (Lin and Rood, 1996), with MECCA (Sander et al., 2011a) providing the source of chemistry integrated into the model. Relevant for representation of heterogeneous chemistry in the stratosphere, deviations from thermodynamic equilibrium are accounted for, which has implications for the distribution of polar stratospheric clouds (PSCs) and associated ozone depletion. In the troposphere, an offline representation of aerosol (dust, sea salt, organic carbon, black carbon, sulphates and nitrates) provides surfaces for heterogeneous chemistry. Lightning NO_x, soil NO_x and isoprene (C_5H_8) are parameterised online for EMAC using the submodel ONEMIS (Jöckel et al., 2016). The model provides a consistent handling of the photolysis and shortwave radiation schemes, with particular regard to the evolution of

the solar cycle (Morgenstern et al., 2017). The Quasi Biennial Oscillation (QBO) is internally generated by the model, although zonal winds near the equator are nudged towards a zonal wind field (Brinkop et al., 2016) with a 58 day relaxation timescale to ensure realistic simulation of the QBO magnitude and phasing (Jöckel et al., 2016). Ozone is tagged as stratospheric in the O_3S tracer simulation above the tropopause as defined by the World Meteorological Organisation (WMO) thermal definition equatorward of 30°N/S and using the 3.5 potential vorticity unit (PVU) dynamical tropopause definition poleward of 30°N/S.

2.1.2 CMAM

Simulations from the atmosphere-only Canadian Middle Atmosphere Model (CMAM) are used here with a T47 spectral resolution (equivalent to ~ 3.75° by 3.75°) on the linear Gaussian grid used for the physical parameterisations in CMAM, with 71 vertical hybrid sigma pressure levels which have extend to 0.01 hPa (~ 95 km altitude) (Hegglin et al., 2014; Pendlebury et al., 2015). The model uses spectral advection of 'hybrid' moisture for transport (Merryfield et al., 2003) and a similar spectral advection of 'hybridized' tracers for chemically active tracers exhibiting strong horizontal gradients (Scinocca et al., 2008). Whilst a representation of heterogeneous chemistry on PSCs is provided, the model does not account for Nitric Acid Trihydrate (NAT) or PSC sedimentation (resulting in denitrification). Heterogeneous chemistry calculations are also made in the troposphere through prescribing sulphate aerosol surface area densities. Chemistry is calculated throughout the troposphere, although the only hydrocarbon considered is methane. To account for isoprene (C_5H_8) oxidation in CMAM, an additional 250 Tg-CO/year in emissions (including an additional 160 Tg-CO/year from soils) is included, distributed as Guenther et al. (1995) isoprene emissions. Unlike EMAC, soil NO_x emissions are not calculated online for CMAM and are instead prescribed, with lightning NO_x emissions parameterised from the Allen and Pickering (2002) updraft mass flux scheme (Morgenstern et al., 2017). Compared with EMAC, consistency in the radiation and photolysis schemes has not specifically been imposed. Although CMAM does not generate a QBO internally, a representation of the QBO is induced in the SD simulations through nudging to ERA-Interim. The stratospheric ozone (O_3S) tracer uses the WMO thermal tropopause definition as the threshold for tagging of ozone as stratospheric across all latitudes, with an additional criterion that the tropopause must be < 0.7 in hybrid-sigma coordinates to prevent erroneous identification at high latitudes, during winter especially.

2.2 Observations

2.2.1 OMI

The ozone monitoring instrument (OMI) is a Dutch/Finnish UV/VIS nadir-viewing solar backscatter spectrometer aboard the NASA-Aura satellite launched in July 2004. The satellite has a retrograde, sun-synchronous polar orbit (inclination of 98.2°) at an altitude of 705 km, providing some 14 orbits a day with a local equatorial crossing time in the ascending node of 13:45 local time (Levelt et al., 2006). OMI operates in the 270-500 nm spectral interval and has a spectral resolution of 0.42-0.63

nm (Foret et al., 2014). OMI is the first of a generation of instruments which use 2-D detector arrays, providing concurrent sampling at all across-track positions, as opposed to platforms which use a 1-D detector array to scan across track. OMI supplements the observational knowledge of ozone from other longstanding satellite platforms, such as NASA's Total Ozone Mapping Spectrometer (TOMS) instrument and ESA's Global Ozone Monitoring Experiment (GOME) instrument, at a much enhanced spatial resolution (e.g. 13 km x 24km for OMI compared with 40 km x 320 km for GOME in the along track and across track directions nominally at nadir). The across track resolution however becomes significantly coarser away from nadir; reaching 13 km x 150 km towards the edge of the swath (corresponding to an angle of 57° from nadir). The swath is 2600 km wide at the surface resulting from a wide field of view of 114º with a near global coverage time of one day (Levelt et al., 2006; Foret et al., 2014). Temperature-dependent spectral structure in the region between 320 and 345 nm (the Huggins Band) contains the information required for retrieval of ozone in the troposphere region (Miles et al., 2015). The logarithm of the ozone volume mixing ratio on a fixed pressure grid (surface pressure, 450, 170, 100, 50, 30, 20, 10, 5, 3, 2, 1, 0.5, 0.3, 0.17, 0.1, 0.05, 0.03, 0.017, 0.01 hPa) provides the basis for the retrieved profiles (Miles et al., 2015).

This study uses 1000-450 hPa (0-5.5 km) subcolumn ozone values retrieved from OMI by the Rutherford Appleton Laboratory (RAL) height-resolved optimal estimation profiling scheme (Miles et al., 2015; Gaudel et al., 2018), for one in four 50 x 50 km samples in every 100 x 100 km bin, which has been further optimised to increase sensitivity to tropospheric ozone. These "Level-2" (L2) data have been averaged into monthly mean 2.5° x 2.5° (~ 275 km) gridded "Level-3" (L3) data between 2005 and 2010. This resolution is more comparable with the resolution of the CCM simulations used in this study for model comparisons (section 3). Validation against ozonesondes for this subcolumn, after applying averaging kernels (AKs) to account for vertical smearing associated with the satellite retrieval, yields a relatively low retrieval bias of ~ 1.5 Dobson Units (DU) (6 %). The sign of the bias is latitude dependent for lower tropospheric ozone – underestimation in the southern hemisphere by ~ 15-20 % (1-3 DU) and overestimation in the northern hemisphere by ~ 10 % (2 DU). These systematic biases can be attributed to inaccuracies in the radiative transfer modelling, which are partially rectified through use of a priori information to shift the erroneous retrieved profiles towards the true values (Mielonen et al., 2015). An additional monthly mean, (linearly interpolated) latitude dependent bias, identified with respect to the global ozonesonde ensemble, was also corrected for in the OMI data used in this study. Other filtering criteria used to enhance the quality of the dataset include omission of observations with a cloud fraction greater than 0.2 and a solar zenith angle exceeding 80°. The 1000-450 hPa (0-5.5 km) OMI subcolumn data is considered a representative approximation of the full tropospheric ozone column amount, due to vertical smearing of information from above 450 hPa (~ 5.5 km). This estimation differs from other techniques such as cloud slicing (e.g. Ziemke and Chandra, 2012) and residual methods such as total column ozone from OMI minus vertical profile measurements from the Microwave Limb Sounder (MLS) (e.g. Ziemke et al., 2011). In comparison with the OMI-MLS method, the OMI-RAL profiling scheme is more (less) sensitive to the lower (upper) troposphere (Gaudel et al., 2018). Therefore to ensure a direct comparison, in order to test the level of agreement with models and ozonesonde observations, averaging kernels (AKs) should be applied to these datasets to induce such smearing of information that inherently occurs in UV-nadir satellite measurements.

The influence of AKs is critically evaluated for the 1000-450 hPa subcolumn for both the models and ozonesondes in section 3.

OMI is regarded as a very stable platform, with the radiometric degradation during the instrument's lifetime estimated to have been just ~ 2 % in the UV and ~ 0.5 % in the VIS channel, which is significantly lower than other comparable instruments (Levelt et al., 2017). Despite this, the quality of radiance data began to decline from 2007 onwards (but particularly starting from 2009) across all wavelengths in a progressively larger number of across-track views, corresponding to rows in the 2-D detector arrays; suspected to be blocked by insulation blankets covering the instruments which have become damaged. This one main anomaly is subsequently referred to as the row-anomaly (Schenkeveld et al., 2017). Although OMI has high sensitivity to the troposphere, sensitivity is much weaker near the surface (Sellitto et al., 2011), with factors such as surface albedo and aerosols in the PBL causing interference (Liu et al., 2010).

2.2.2 Ozonesondes

Vertical ozone profile data over the period 1980-2010 was derived from the World Ozone and Ultraviolet Radiation Data Centre (WOUDC); an archive of balloon-borne in situ measurements of ozone, together with other variables such as temperature, humidity and pressure. Ozonesondes typically provide a vertical resolution of ~ 150 m from the surface up to a maximum altitude of approximately 35 km, although not in all cases (Worden et al., 2007; Nassar et al., 2008). Most sonde stations launch ozonesondes on a weekly basis, but a number of European sites provide measurements 2-3 times a week (Worden et al., 2007). The WOUDC archive contains measurements from three different instruments: the Brewer-Mast (BM), the electrochemical concentration cell (ECC) and the Japanese ozonesonde (KC) (SPARC, 1998). The vast majority of the WOUDC sonde profile measurements were however obtained from ECC ozonesondes, although all three instruments yield measurements of ozone equivalently (in units of partial pressure using atmospheric pressure as a vertical coordinate) through detection of the oxidation reaction between ozone and potassium iodide (KI) in an aqueous solution (Komhyr et al., 1995; WMO, 1998). Differences can however arise due to instrument type (two different manufacturers), procedures and the strength of the KI solution (Thompson et al., 2003; 2007). The accuracy of sonde measurements is typically estimated to be within the range of ± 5 %, depending on various factors. Precision between the various sonde types is estimated to be within ± 3 %, with systematic biases of less than ± 5 % within the lower to middle stratosphere (12-27 km altitude range), provided that profile measurements have been normalised with respect to ground based total ozone measurements (WMO, 1998).

Uncertainties are however much larger in the troposphere due to lower concentrations of ozone, yielding a relatively low signal-to-noise ratio, which increases the susceptibility to both instrumental errors and instrumental variability. Sonde performance can additionally be affected by local air pollution, which can further enhance the level of uncertainty. Systematic differences between different instruments in the troposphere were estimated to vary between 10 and 15 % in various

intercomparison campaigns between 1970 and 1990. There is evidence that the ECC sondes have greater precision and consistency than either the BM or KC sondes here (e.g. WMO-III, JOSIE campaigns); precision of ± 5-10 % for ECC compared with a range of 10-20 % for BM/KC. A small positive bias of 3 % is noted for ECC with no evidence of biases exceeding ± 5 % for BM/KC.

3. Tropospheric Ozone (Model-Measurement Comparison)

In order to evaluate the utility of the models in assessing tropospheric ozone and estimating stratospheric influence, the CCM simulations (EMAC and CMAM) are first validated here against the OMI observations, in addition to the spatially and temporally limited height resolved ozonesonde measurements. This is achieved through a combined model-measurement characterisation of the seasonal and geographical variability of tropospheric ozone (section 3.1), together with the interannual variability (section 3.2) over the 2005-2010 period. Lastly, a vertically resolved assessment of the CCMs is provided for three different mid-latitude regions (Europe, eastern North America and the Tasman Sea) from combined ozonesonde profile measurements between 1980 and 2010 (section 3.3).

Seasonal composites of monthly mean 1000-450 hPa (0-5.5 km) subcolumn ozone from OMI, together with available ozonesonde-derived AK-fitted subcolumns, and the respective differences for each AK-fitted CCM are shown in Fig. 1. A seasonal maximum in tropospheric ozone is evident in each hemisphere during spring, which is more pronounced in the Northern Hemisphere and extended in many regions through to summer (JJA). In contrast to the extratropics, tropospheric ozone remains low year-round (< 20 DU) at low-latitudes although some seasonality is apparent; notably a northward (southward) shift in the region of lowest ozone from boreal winter (summer) into summer (winter). This is likely associated with the seasonal migration of the Inter Tropical Convergence Zone (ITCZ) which closely follows the region of maximum solar insolation. In this region, strong upwelling occurs which leads to the transport of ozone depleted air from the tropical PBL upwards towards the tropopause. This is most pronounced across the Maritime Continent where convective activity is climatologically most intense (e.g. Thompson et al., 2012).

The BDC, which leads to meridional transport in ozone and other constituents in the stratosphere, is strongest (weakest) during winter (summer) and it is this annual variability which primarily governs the seasonality of tropospheric ozone (through changes in STE) in regions of the extratropics where emissions of tropospheric ozone precursors are at a relatively low background level (Roscoe, 2006). This is invariably the case across much of the Southern Hemisphere, where anthropogenic precursor emissions are substantially lower and more spatially confined in comparison with the Northern Hemisphere. In some regions such as the South Atlantic, it is evident that tropospheric ozone is similarly high in winter (JJA) (~ 25-30 DU) but it is known that this is a result of biomass burning activity in western Africa and resultant plumes which are advected offshore during the dry season in particular (e.g. Mauzerall et al., 1998). Across Antarctica and the Southern Ocean however, halogen-

Atmos. Chem. Phys. Discuss., https://doi.org/10.5194/acp-2018-1026
Manuscript under review for journal Atmos. Chem. Phys.
Discussion started: 30 October 2018

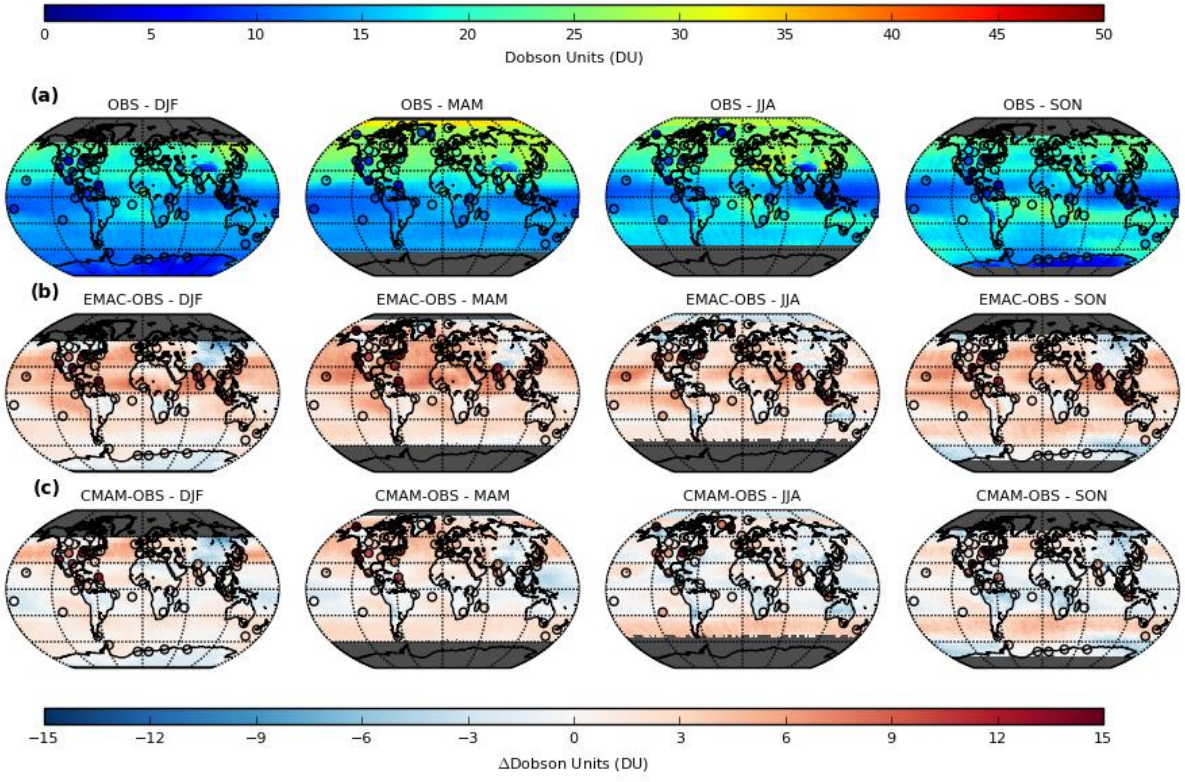

Figure 1 – Seasonal composites of monthly averaged 1000-450 hPa (0-5.5 km) subcolumn O_3 (DU) for 2005-2010 (left to right) from (a) OMI, (b) EMAC minus OMI and (c) CMAM minus OMI. Circles denote (a) equivalent ozonesonde-derived subcolumn O_3 (DU), (b) EMAC minus ozonesonde difference and (c) CMAM minus ozonesonde difference. All data was regridded to 2.5° resolution (~ 275 km). All model and ozonesonde subcolumn data has been modified using AKs to ensure a direct comparison.

induced stratospheric ozone depletion is the dominant driver of the seasonality; leading to a minimum in spring (SON), although no observations from OMI are available during the polar night (MAM and JJA). In the Northern Hemisphere, the strong influence of emission precursors from widespread anthropogenic activity serves to delay and broaden the maximum, since the peak in the in situ photochemical formation of ozone is driven by solar insolation. This is particularly apparent in subtropical regions such as in the eastern Mediterranean due to favourable photochemical conditions for the production and subsistence of ozone during the summer months.

A corresponding zonally averaged monthly mean evolution, together with the respective differences for each CCM (both with and without AKs) is additionally shown in Fig. 2 and further summarised as 30° latitude band averages in Table S1. Whilst

Atmos. Chem. Phys. Discuss., https://doi.org/10.5194/acp-2018-1026
Manuscript under review for journal Atmos. Chem. Phys.
Discussion started: 30 October 2018

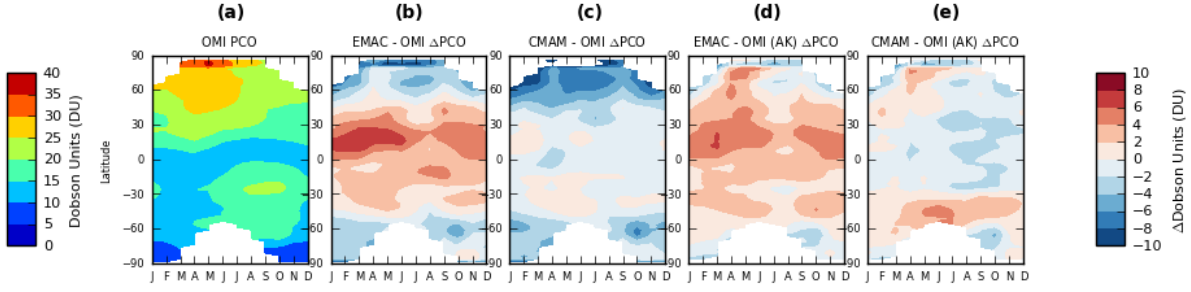

Figure 2 – Zonal-mean monthly averaged 1000-450 hPa (0-5.5 km) subcolumn O_3 (DU) for 2005-2010 from (a) OMI, (b) EMAC minus OMI without AKs, (c) CMAM minus OMI without AKs, (d) EMAC minus OMI with AKs and (e) CMAM minus OMI with AKs.

the AK-fitted EMAC differences with respect to OMI (Fig. 1 and Fig. 2d) show an overall year-round, albeit seasonally varying positive bias, particularly within the 0° to 30° latitude band (~ +2-8 DU), the difference is largely negative in CMAM (~ 0 to -4 DU), except during spring (MAM) in parts of the Northern Hemisphere (~ 0 to +4 DU) and within the 30°S to 60°S latitude band (~ +2-6 DU). Although such differences on a zonally averaged basis are relatively small (on the order of 10-20 %), the systematic nature and seasonal dependence of such biases is important to consider. Regional differences are evidently larger however, with differences of up to 10 DU (50 %), such as over mid-latitude oceanic regions where both CCMs show a positive bias relative to OMI and also with respect to limited available ozonesonde data from maritime locations. Some continental regions such as eastern Asia on the other hand show a negative bias in most seasons; largest in winter (DJF) (5-10 DU or 20-40 %). A recent study by Hoesly et al. (2018) shows discrepancies between the CMIP5 NOx emissions database and an updated, refined database over the timeframe considered, which could explain the pattern of biases between the continental regions of the Northern Hemisphere. The sign of the biases is more complex and spatially variable in summer (JJA) but are typically low (-3 to +3 DU), implying that the CCMs are reasonably consistent overall with the OMI measurements during this season. In the Southern Hemisphere, the general positive bias is weaker (particularly in austral winter and spring) and most regions show a negative bias in at least one season. Model-measurement agreement here is typically higher compared with the Northern Hemisphere, particularly for latitudes where O_3 precursor emissions are lower and in the less photochemically active seasons (i.e. autumn and winter). This could indicate that CCMs include excessive emissions in the Northern Hemisphere particularly (Young et al., 2013; Shepherd et al., 2014) or that the role of tropospheric sinks (e.g. through wet and dry deposition or other loss reactions) is underestimated (Revell et al., 2018), with our results indicating regionally differing magnitudes in these biases.

Both Fig. 2 and Table S1 show the importance of applying AKs (on a monthly mean zonally-averaged basis) in order to diagnose the agreement between the two datasets, since it is clear that both CCMs significantly underestimate the amount of

tropospheric ozone overall at both middle and high latitudes, relative to the OMI observations. The effect of applying the AKs (Fig. 2d-2e) is shown to significantly reduce or even eradicate the negative bias (poleward of 30ºN/S), and it is this difference which indicates the approximate magnitude of the influence vertical smearing has on the retrieved OMI subcolumn measurements. A residual negative bias (~ -2 to -6 DU) also exists in the Southern Hemisphere during spring (SON) over the Southern Ocean south of 60°S (adjacent to Antarctica). This could reflect greater stratospheric influence than captured by the models (particularly EMAC) or perhaps more likely an offset in jet stream positioning, as supported by the zonally-structured positive bias northward of 60°S, which strongly influences both STE and long-range transport. Biases in much of the tropics appear also to be connected to dynamics which favour long-range transport (e.g. trade wind circulations) originating from regions of known precursor emissions (e.g. biomass burning from South America).

Differences with AKs show that EMAC is in slightly better agreement with OMI across the Southern Hemisphere extratropics, although CMAM is in closer or comparable agreement over the tropics and the Northern Hemisphere. The model is especially consistent during JJA and SON over the continents in particular (Fig. 1b and 1c). Furthermore, a high level of agreement between the ozonesonde and OMI observations is apparent in all four seasons, confirming that the OMI retrieval algorithm correctly captures the regional and seasonal climatological features in tropospheric ozone. Some sonde sites however show consistently smaller amounts of ozone (e.g. western North America and Greenland), although this may be attributed to the high elevation (e.g. mountain summit locations) of these sites, relative to the average topographical elevation of a 2.5º grid cell within which the OMI observations are averaged over, which inherently leads to lower amounts of ozone within the partial column.

3.2. O_3 Interannual Variability

As a metric of interannual variability, seasonal aggregates of the computed relative standard deviation (RSD) of the monthly mean O_3 for both OMI and each CCM are shown in Fig. 3. Variability in the tropics is enhanced due to the significantly lower mean tropospheric ozone, in comparison with the extratropics. Although OMI shows much higher variability than the models, there is good agreement in regions of high RSD across much of the tropics (> 10 %), which is largest during SON, at least from the OMI observations. The highest RSD is consistently found over the western Pacific and the Maritime Continent close to the equator, where it approaches 20 % for both OMI and the CCMs (particularly CMAM). The region is strongly influenced by some of the main drivers of natural variability, including the El Niño Southern Oscillation (ENSO) and the Madden Julian Oscillation (MJO). Throughout the tropics, high variability may also be associated with the Quasi Biennial Oscillation (QBO). Although the QBO is a stratospheric phenomenon, studies show that the alternating phases of the zonal equatorial wind can influence tropospheric ozone by as much as 10-20 % (~ 8 ppbv) (e.g. Lee et al., 2010). The RSD is generally lower for OMI outside of the tropics, although significant variability (> 10 %) is still evident for some regions in different seasons. The CCMs in contrast show very low RSD over much of the extratropics (< 5 %), with only subtle spatial structures evident in the seasonal

Atmos. Chem. Phys. Discuss., https://doi.org/10.5194/acp-2018-1026
Manuscript under review for journal Atmos. Chem. Phys.
Discussion started: 30 October 2018

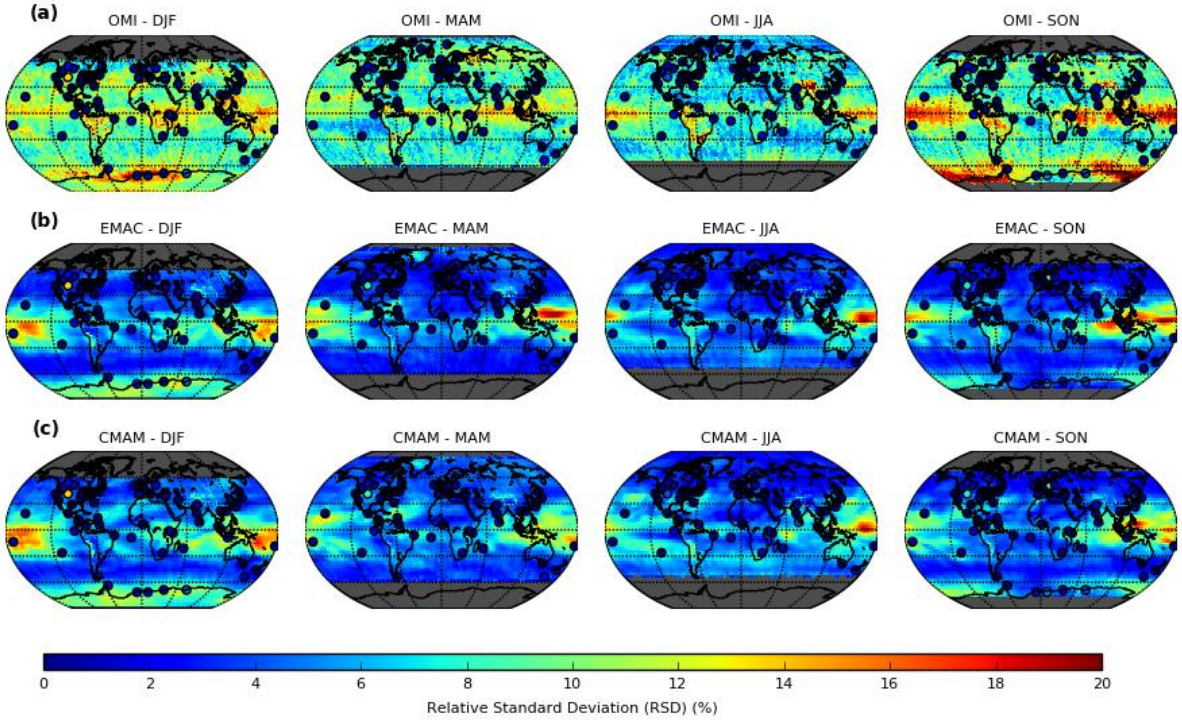

Figure 3 – Seasonal composites (left to right) of monthly 1000-450 hPa (0-5.5 km) subcolumn O_3 relative standard deviation (RSD) (%) for 2005-2010 for (a) OMI, (b) EMAC and (c) CMAM. RSD calculated as the standard deviation (SD) divided by the mean (multiplied by 100). Circles denote (a-c) the seasonal RSD calculated from ozonesonde measurements. Model and ozonesonde subcolumn data has again been modified using AKs to ensure a direct comparison.

composites. Equivalent composites of the absolute standard deviation (SD) (not shown) show some variability however at mid-latitudes during winter and spring in each hemisphere (up to 2 DU), principally in oceanic regions, and this may indicate sensitivity to the main extratropical cyclone tracks. Higher RSD is however shown across Antarctica during polar day and over the Southern Ocean (up to 10 %), which is collocated in the corresponding OMI seasonal composites. This may largely be a retrieval artefact caused by vertical smearing, which is highly dependent on the tropopause height, since comparative RSD fields from the CCMs without AKs show no such structure (not shown).

3.3. O_3 Vertical Distribution Assessment

To evaluate the vertical agreement of the CCM O_3 VMR tracer simulations, monthly mean ozonesonde-derived measurements were interpolated and averaged between ±20 hPa of the 22 different model pressure levels between the surface (~ 1000 hPa)

Atmos. Chem. Phys. Discuss., https://doi.org/10.5194/acp-2018-1026
Manuscript under review for journal Atmos. Chem. Phys.
Discussion started: 30 October 2018

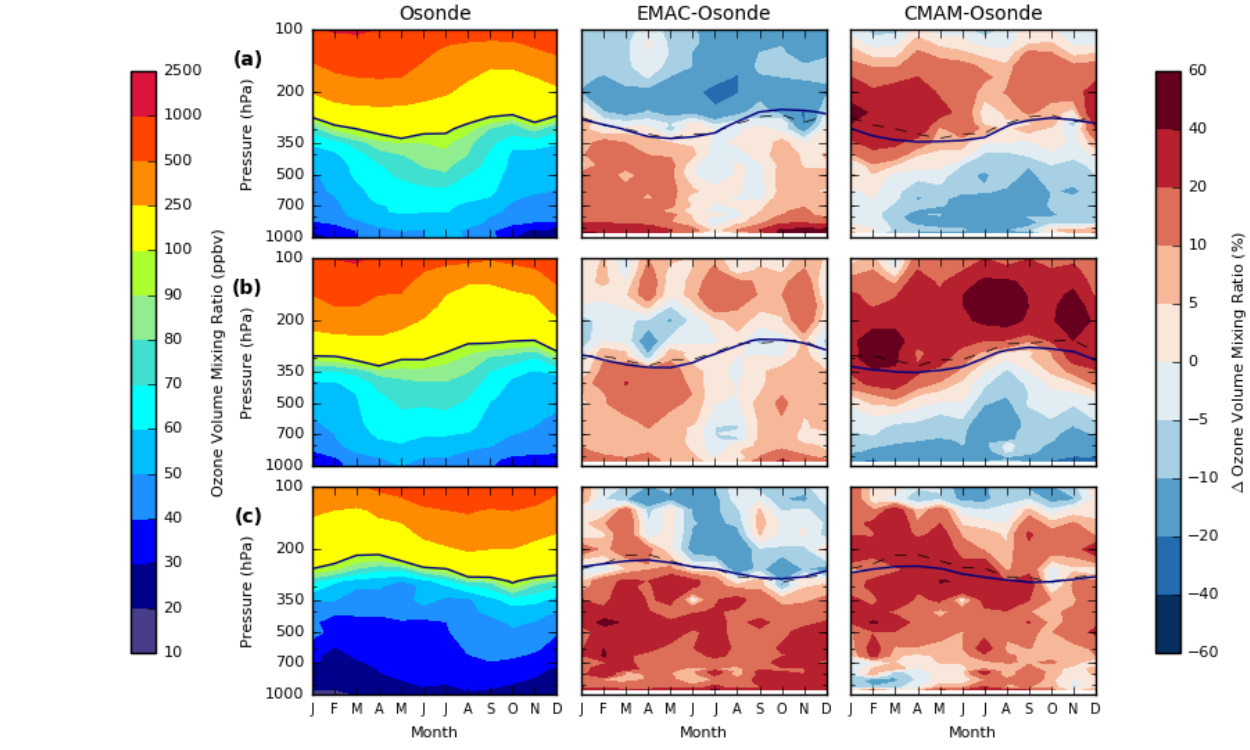

Figure 4 – Monthly evolution of the vertical distribution of mean O_3 volume mixing ratio (VMR) (ppbv) derived from ozonesonde measurements (left column); EMAC minus ozonesonde differences (%) (middle column) and CMAM minus ozonesonde differences (%) (right column) over the period 1980-2010 inclusive for three different world regions: (a) Europe (n = 18), (b) eastern North America (n = 14) and (c) Tasman Sea (n = 6). The ozonesonde/model 100 ppbv contour (the ozone defined extratropical tropopause as identified in Bethan et al. (1996)) is additionally highlighted in bold (ozonesonde 100 ppbv contour indicated again by dashed line – middle and right column).

and the lower stratosphere (100 hPa) for three different extratropical regions. Fig. 4 (Fig. S1) shows the monthly mean evolution averaged over all sites (left), together with the respective percentage (ppbv) differences relative to the nearest model grid columns in EMAC (middle) and CMAM (right), within each bounding boxes (region): (a) Europe (30° N - 65° N, 15° W - 35° E), (b) eastern North America (32.5° N - 60° N, 92.5° W - 55° W) and (c) the Tasman Sea (55° S - 15° S, 140° E - 180° E). Tables S2a-c additionally provides a summary of this information on a seasonal basis for six selected pressure levels for each region. These regions were selected for the assessment due to the relatively high number of ozonesonde sites in close proximity. Furthermore, the variability in emissions of ozone precursors and stratospheric influence due to varying UTLS dynamics in these predominantly extratropical regions, make these regions suitable for evaluating the realism to which the CCMs simulate these influences.

The seasonality in ozone concentration is shown to be very similar in both Europe and eastern North America as expected for two regions of similar latitude in the same hemisphere. In the stratosphere, a springtime maxima (autumn minima) is clear, although the timing is not synchronous at all pressure levels, with a tendency for a delayed maximum (minimum) in each region with increasing pressure (decreasing altitude). This is also apparent for the Tasman Sea region, albeit the seasonality is reversed. This can be attributed to the BDC in the lower stratosphere, which leads to a gradual accumulation of ozone during wintertime in the lowermost stratosphere and a subsequent gradual depletion of ozone during summertime as the circulation weakens (Holton et al., 1995; Logan et al., 1985; Hegglin et al., 2006). For all regions, this delayed signal in the maximum (minimum) in ozone concentration propagates down into the troposphere (identified here as the region < 100 ppbv), with the exception of the springtime maximum over the Tasman Sea which peaks earlier with increasing pressure from the tropopause (around late September) towards the surface (early August). Clearly though, there is a large difference in the climatological ozone concentration throughout the year between this region and both Europe and eastern North America; the Tasman Sea region reflecting only a very limited influence from emission precursors. The composite produced for this region likely provides a reasonable representation of the natural background influence of the stratosphere on tropospheric ozone in the extratropics, in contrast to the other two regions.

The computed model-ozonesonde monthly mean differences reveal notable differences both between each model and each region in the troposphere (~ 300-1000 hPa); as high as 20-30 ppbv (> 50 %) between each model in the lower troposphere over Europe and between both eastern North America and the Tasman Sea in the lower troposphere in CMAM. EMAC shows an almost universal positive bias between 0 and 40 % (0-20 ppbv) throughout the year for all three regions which contrasts with the overall negative bias in the stratosphere (~ 100-300 hPa) (except over eastern North America). Some seasonal dependence in the bias is evident over Europe and eastern North America, with the largest (smallest) difference between January and May (June and August). A less pronounced secondary peak in the magnitude of the bias is also evident during autumn (SON). An exception to this is in the lower troposphere (> 850 hPa) over Europe, where the largest differences are evident (~ +20-60 % equating to some +10-20 ppbv) from autumn (SON) through to spring (MAM). In contrast, no obvious seasonal variation in the bias is apparent over the Tasman Sea region. For CMAM, a generally negative, seasonally dependent bias (~ 5-20 % or 5-10 ppbv) is apparent in the lower to middle troposphere over Europe and particularly eastern North America, most pronounced during summer (JJA), whereas an overall positive bias (up to 10-40 % or 5-20 ppbv) exists over the Tasman Sea, largest in the free troposphere. Both the seasonal character of the negative bias over Europe and eastern North America (largest during the most photochemically active months), together with the difference in the sign of the bias between the troposphere and the UTLS, strongly implies a difference in the implementation of the tropospheric chemistry scheme in CMAM compared with EMAC since prescribed emissions should be equivalent in each model. Specifically, the omission of non-methane VOCs (NMVOCs) in CMAM likely accounts for much of this underestimation.

The largest absolute differences are however indeed evident in the lower stratosphere (100-300 hPa), with a systematic positive bias in CMAM in most seasons (widely between +50 and +200 ppbv, ranging from 10-50 %). A slight negative bias (~ -10 to -50 ppbv or -0-10 %) is however apparent between 100 and 150 hPa over Europe, largely during summer (JJA), and also more pronounced over the Tasman Sea from March through to November (> 50 ppbv or 5-20 %). Over eastern North America, a very large positive bias is evident in CMAM throughout the year ranging between 20 and 60 % (+50 to +200 ppbv), with a seasonal shift in the height of the largest differences, similarly to over Europe yet more pronounced. In contrast, the differences between EMAC and the ozonesonde measurements have a very different character, with a general negative bias over Europe, particularly in summer (JJA) (~ -20 to -100 ppbv or -10-20 %). Over eastern North America and the Tasman Sea, the pattern and magnitude of the biases is more complex with both pressure (altitude) and month. An overall positive bias is found over eastern North America (typically +20 to +50 ppbv or +5-20 %), except from January to May between ~ 170 and 250 hPa, whilst an overall negative bias (generally between -20 and -50 ppbv or 5-20 %) is evident over the Tasman Sea except between January and May and for a small region (120-180 hPa) during August-September. The general negative bias in EMAC (positive bias in CMAM) might indicate an underestimation (overestimation) in the strength of the BDC but the seasonal dependence of the bias, and in particular the complexity in EMAC, suggests influence from other factors.

3.4 Summary

In summary, the CCM simulations are broadly in agreement with both sets of observations, capturing both the extent and magnitude of geographical and seasonal features in tropospheric ozone over the concurrent period of data availability (2005-2010). There is very close agreement overall in the global mean seasonal composites of tropospheric subcolumn (1000-450 hPa) ozone between each CCM, although differences relative to OMI show that there is an overall significant, systematic positive bias in the EMAC (Fig. 1 and 2), particularly over the Northern Hemisphere (~ 2-8 DU), whereas no overall bias is apparent in CMAM despite some meridional and seasonal differences (~ -4 to +4 DU). An evaluation of the model-ozonesonde differences in the vertical distribution of ozone volume mixing ratios (ppbv) over both Europe and eastern North America (Fig. 4) indicates a different origin for the biases in each model compared with OMI. In EMAC, the positive bias is predominantly a result of excess in situ photochemical production from emission precursors, whereas biases in CMAM are largely determined by the relative influence of excessive vertical smearing of ozone (induced by applying the OMI AKs). This results from a large positive ozone bias in the lower stratosphere (not present in EMAC), as well as the much more conservative tropospheric chemistry scheme implementation. The additional smearing from AKs is concluded to overcompensate for the reduced in situ production of ozone to yield a larger positive or comparable bias in CMAM (poleward of 30°S/N), where the application of AKs has a disproportionally larger effect on the estimated subcolumns. In contrast, a larger positive bias is found in EMAC over low latitudes (30°N-30°S), but primarily in the North Hemisphere where precursor emissions are more abundant, since vertical smearing of information is far more limited due to a higher tropopause. The zonal average monthly mean integrated subcolumn OMI-model differences without AKs (figure 2b-c) would be consistent with this interpretation and it is obvious

that application of the OMI AKs must induce additional vertical smearing of ozone in CMAM in the equivalent latitude range (~ 30-65°N) compared with EMAC (figure 2d-2e) due to the presence of a high ozone bias in the lower stratosphere compared with both ozonesondes and EMAC. Such factor is also suspected to be influential in also explaining the transition from a negative to a positive bias after applying AKs in the Southern Hemisphere between May and December in the region between 30°S and 60°S in CMAM. It is known that CCMs tend to have inherent biases in ozone in the lower stratosphere (e.g. Jöckel et al., 2006, 2016; Pendlebury et al., 2015; Kolonjari et al., 2017), so it is likely that the results found here are applicable hemisphere-wide but again further investigation is warranted. The interannual variability (Fig. 3) in the models seems to be consistent with that from the OMI measurements and reported in the literature, at least in the equatorial region where the magnitude of interannual variability is typically on the order of ~ 10-20 %. In the extratropics, both ozonesondes and models show smaller variability (< 5 %), in contrast to OMI. Whether such differences arise due to model inadequacies in capturing the magnitude of natural variability, or simply as a result of measurement noise in the OMI observations is a subject for further investigation.

4. Stratospheric Influence

Having assessed the ability of the CCMs to represent key features of the global climatology of tropospheric ozone with respect to both in situ and satellite observations, model simulations of the vertical distribution in ozone concentration are now investigated globally over the 1980-2010 climatological period, together with the role of stratospheric ozone in influencing both regional and seasonal variations.

4.1 O_3 Vertical Distribution, Seasonality and Stratospheric Contribution (O_3F)

Seasonal composites of the monthly mean, zonal-mean vertical distribution of ozone concentration (O_3S concentration) (VMR) in the troposphere and lower stratosphere (1000-80 hPa) are shown in Fig. 5 (Fig. S2) for EMAC (a), CMAM (b) and CMAM-EMAC (c), together with the percentage contribution of mean ozone of stratospheric origin (O_3F: dashed lines). The meridional distribution in the tropospheric seasonal mean ozone concentration corresponds closely to the latitudinal variability in the integrated 1000-450 hPa subcolumn seasonal composites produced from both the CCM and OMI data (Fig. 1 and 2). The highest concentrations of ozone according to both CCMs can be found over mid-latitudes, with consistent seasonality to that identified in section 3; a maximum in the Northern Hemisphere during spring into summer (MAM and JJA) and in spring (SON) over the Southern Hemisphere. It is obvious that the concentration of ozone is significantly greater year-round in the Northern Hemisphere. This is due in part to the large difference in precursor emissions from the surface but also due to a stronger BDC in the Northern Hemisphere and subsequent enhanced STE of ozone, with the former (latter) clearly a greater influence near the surface (upper troposphere). As indicated by the dashed contours, the stratospheric influence increases with altitude for all latitudes across all seasons. However, there is a significant meridional gradient in the stratospheric influence,

Atmos. Chem. Phys. Discuss., https://doi.org/10.5194/acp-2018-1026
Manuscript under review for journal Atmos. Chem. Phys.
Discussion started: 30 October 2018

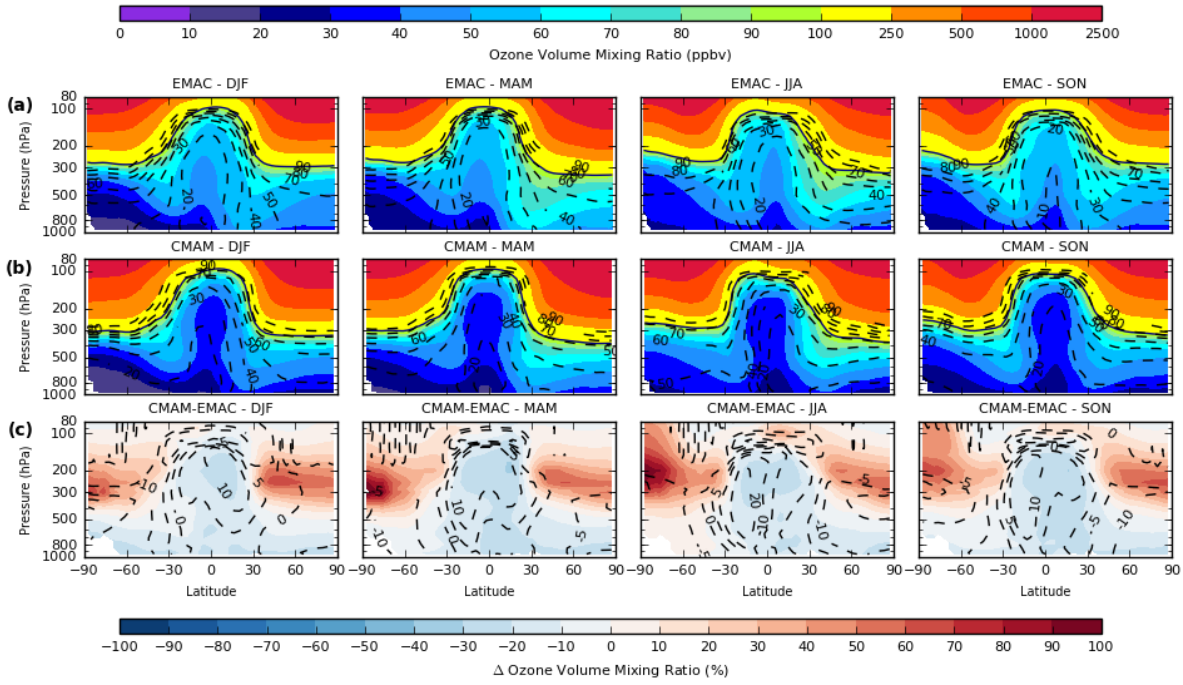

Figure 5 – Zonal mean seasonal composites of monthly mean O_3 concentration (ppbv) for the troposphere and lower stratosphere (1000-80 hPa) from (a) EMAC, (b) CMAM and (c) CMAM and EMAC (CMAM-EMAC) percentage differences over the period 1980-2010. Dashed lines indicate the stratospheric contribution (%) calculated using both ozone tracers in each model: O_3F (%) = (O_3S / O_3) x 100. The 100 ppbv contour (bold line) is included as a reference for the tropopause altitude (top and middle row).

with values ranging from < 30 % over the tropics in all four seasons throughout the troposphere, to maximum values between 40 and 75 % during the winter months at high latitudes in both hemispheres from the surface to 350 hPa. Towards summertime, this fraction decreases sharply across middle and high latitudes (particularly near the surface) due to a combination of reduced STE and increasing importance of precursor emissions during the photochemically active months. Thus in relative terms, the stratosphere has a smaller contribution outside the winter months (lowest in summer). Despite this, the stratosphere has the largest contribution during spring in absolute terms (see supplement Fig. S2), extended through to summer in the Northern Hemisphere upper troposphere, which is well established in the literature (e.g. Richards et al., 2013; Škerlak et al., 2014; Zanis et al., 2014). This further implies that the influence of the stratosphere becomes secondary to precursor emissions during the photochemically active months, away from the upper troposphere.

The inter-model difference in the zonal mean ozone concentration for each season is shown in Fig. 5 (c). With respect to EMAC, CMAM shows lower values overall throughout the tropical troposphere, and also over the Northern Hemisphere lower and middle troposphere in all seasons (~ 0-30 % or between 0 and -20 ppbv). In contrast, CMAM shows much higher values

in the extratropical upper troposphere (up to +50 ppbv or 50-100 % in relative terms) in all seasons, with smaller positive differences extending towards the surface in the Southern Hemisphere, particularly in winter (JJA). The large difference in the extratropical upper troposphere, in conjunction with the vertically extensive negative bias in the tropics, may be partially attributed to a difference in the large scale dynamics in each model. Notably, a modest downward shift in the height of the extratropical tropopause would lead to such large differences apparent in Fig. 5, due to the existence of a very sharp gradient in ozone concentration at this boundary, Indeed, it has been identified previously that tropopause pressures in EMAC are lower than CMAM (by as much as 30-50 hPa) in free running simulations, equating to a smaller total mass of the lowermost stratosphere (Hegglin et al., 2010), although the actual difference is likely smaller in the case of the specified dynamics simulations analysed here. Apart from over the Southern Hemisphere high latitudes, the negative difference in CMAM (relative to EMAC) throughout much of the troposphere would appear to be related to both a difference in the implementation of the tropospheric chemistry scheme in each model and the amount of simulated O_3S, which is evidently some 0-10 ppbv (up to 20 %) lower in CMAM despite a much larger ozone burden in the extratropical UTLS region (Fig. S2c). An exception to this is over the Southern Hemisphere subtropics during wintertime (JJA) especially where a significantly larger amount of O_3S (~ 0-20 %) is transported down towards the surface in CMAM compared with EMAC (indicative of greater STE). The absence of a positive difference in Fig. 5c in this region however suggests an overwhelming influence of the reduced in situ photochemical formation of ozone in CMAM due to the simplicity of the tropospheric chemistry scheme in this model, despite an obvious larger stratospheric ozone fraction here (O_3F > 20 % larger in CMAM in the mid-troposphere).

4.2 O_3F Global Distribution and Seasonality

The global distribution of ozone of stratospheric origin is next investigated, in order to quantify the relative contribution to tropospheric ozone, as well to help identify preferential pathways of stratosphere-troposphere transport. The climatological fraction of stratospheric sourced ozone (O_3F) is shown globally for EMAC and CMAM, together with the difference between both models (CMAM-EMAC) in Fig. 6 at (a) 350 hPa, (b) 500 hPa and (c) 850 hPa for both DJF and JJA (see Fig. S3 for MAM and SON) over the period 1980-2010, when O_3F reaches a maximum (minimum) in the respective winter (summer) hemisphere. Both CCMs are broadly consistent at each pressure level, with a clear decrease in the O_3F towards the surface as already indicated in Fig. 5. The meridional gradient is largest in the upper troposphere at 350 hPa with low values across the tropics (< 40 % between 30°N and 30°S) associated with both convective upwelling and the short photochemical lifetime of ozone in the tropics, with higher values in the extratropics but particularly in the winter hemisphere (> 70 %). In the Northern Hemisphere mid-latitudes where the gradient is largest, a planetary-scale wave pattern is evident (particularly at 350 hPa) which is consistent with longitudinal variability in the climatological positioning of the upper level jet streams induced by orography (e.g. the Rocky Mountains in North America) (Charney and Eliassen, 1949; Bolin, 1950), particularly in winter (DJF). Although the O_3F is relatively high during summer in each hemisphere at 350 hPa as well, the O_3F is much lower at 500 hPa and 850 hPa (which is consistent with Fig. 5) and reflects the relative minimal role of the stratosphere during this

Atmos. Chem. Phys. Discuss., https://doi.org/10.5194/acp-2018-1026
Manuscript under review for journal Atmos. Chem. Phys.
Discussion started: 30 October 2018

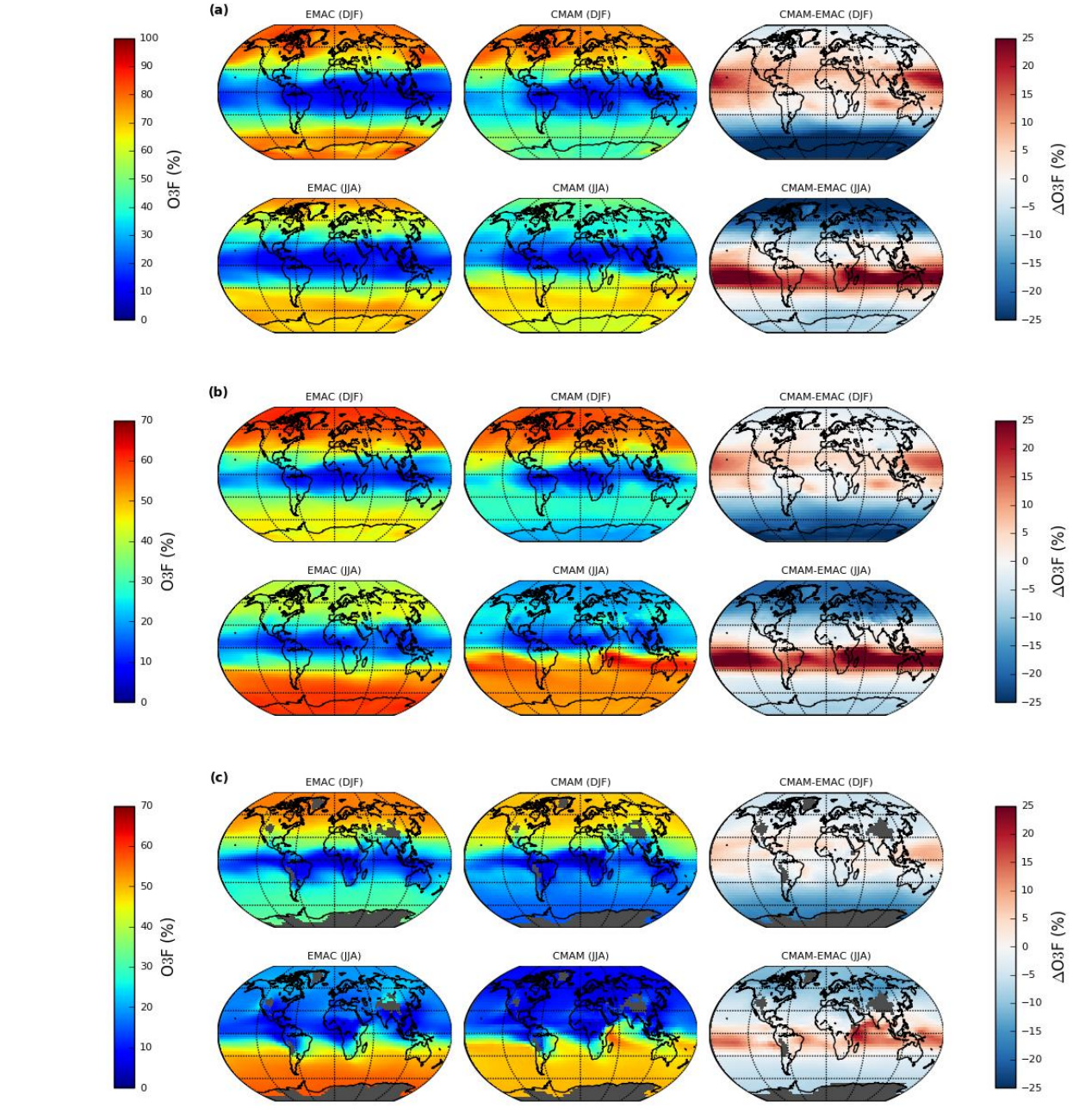

Figure 6 – Seasonal (DJF/JJA) composites of (a) 350 hPa, (b) 500 hPa and (c) 850 hPa monthly mean stratospheric ozone fraction (O_3F) for EMAC (left), CMAM (middle) and CMAM-EMAC (right) over the period 1980-2010. Note the scale difference between (a) and (b-c).

season (with strong influence from precursor emissions instead). At 850 hPa, the stratospheric influence is typically largest over oceanic regions which further reflects the importance of emission precursors over continental regions, particularly in the Southern Hemisphere where biomass burning is prevalent over Africa and South America.

Large differences in O_3F are apparent at high latitudes (poleward of 60°N and 60°S) during summer in each hemisphere at 350 hPa, with CMAM showing a significantly smaller fraction in ozone of stratospheric origin (~ 40-50 %) compared with EMAC (~ 70-80 %). This is despite a positive bias of ~ 20-50 % (20-30 ppbv) in the seasonal mean ozone VMR in CMAM compared with EMAC (Fig. 5c), although this bias exists across all seasons whereas the O_3F bias is seasonally dependent. Inspection of model tracer values (not shown) indicates slightly lower stratospheric ozone (O_3S) in CMAM compared with EMAC, along with higher O_3 values (ozone of non-stratospheric origin) at 350 hPa which gives rise to this difference; although the exact origin of this discrepancy would require further investigation. During wintertime in the Southern Hemisphere (JJA) subtropics, a large positive difference in O_3F also exists over a relatively narrow latitude range between 0°S and 30°S, which is indicative of an equatorward displacement in the position of the subtropical jet stream in CMAM compared with EMAC. The differences show some variation longitudinally, with the largest differences extending from east Africa towards Indonesia and northern Australia and out across the South Pacific. Reference to seasonal composites of the model O_3S VMR tracer (Fig. S2) confirms that the positive bias is related to larger STE in CMAM relative to EMAC, at least over the Southern Hemisphere subtropics. The effect of greater STE, even locally across this latitude range, in CMAM would propagate eastwards due to the influence of upper level winds, leading to transport of ozone-rich air on intercontinental scales. Both the highest O_3S (not shown) and O_3F values in CMAM are apparent over a relatively small geographical area of the Indian Ocean north of Madagascar (adjacent to the east African coastline) which signifies preferential stratosphere-to-troposphere transport in this region which extends deep into the lower troposphere (O_3F > 50 % at 850 hPa). Although EMAC shows relatively high O_3F in the wider region during this season, evidence of a preferential STE pathway here is lacking in this model and indeed no such feature has been widely recognised in the literature. Such differences are non-existent during DJF, although CMAM shows generally higher O_3F over part of the Indian Ocean and the South Pacific and relatively lower O_3F over South America, the South Atlantic and over Africa. The differences described at 350 hPa are very similar at 500 hPa, albeit the negative difference at high latitudes during summer is lower (~ 10-20 %). Although the spatial distribution of the biases is broadly consistent at 850 hPa as well, there is much greater variability regionally in the tropics and the negative bias at high latitudes is relatively low (> 10 %).

4.3 Monthly Evolution of Stratospheric Influence

The zonal-mean monthly evolution of mean ozone (O_3) concentration at 350, 500 and 850 hPa is shown in Fig. 7 based on the aggregated available global measurement network of in situ ozonesonde observations (a), from EMAC (b), and subsequently for EMAC O_3S (c) and EMAC O_3F (d).The ozonesonde measurements are in broad agreement with that simulated by EMAC (and CMAM; see Fig. S4), in terms of both the seasonality and meridional variability in the climatological mean ozone

Atmos. Chem. Phys. Discuss., https://doi.org/10.5194/acp-2018-1026
Manuscript under review for journal Atmos. Chem. Phys.
Discussion started: 30 October 2018

concentration at each of the three different pressure levels. However, the ozone concentration across the Northern Hemisphere high latitudes at both 500 and 850 hPa during the broad spring and summer maximum is somewhat higher (~ 0-10 ppbv) in EMAC, whereas closer agreement with the ozonesonde climatology is apparent for CMAM (Fig. S4). At the 350 hPa level on the other hand, CMAM overestimates ozone in the extratropics relative to both EMAC and ozonesondes by as much as 10-20 ppbv, which is consistent with the identified high ozone bias in the UTLS in CMAM over three different extratropical regions in section 3 (Fig. 4), whereas EMAC is in closer agreement with the ozonesonde-derived composites. Furthermore, there is very high variability with latitude in the tropics compared with EMAC (and CMAM), although this is almost certainly an artefact of both the paucity and poor spatial representativeness of ozonesonde stations. This figure is similar to that produced by Lamarque et al. (1999, Fig. 2., p. 26368) and their model results bear some resemblance to Fig. 7 (Fig. S4) in terms of the characterisation of the zonal mean evolution of ozone VMR and calculated O_3F, although significantly higher concentrations

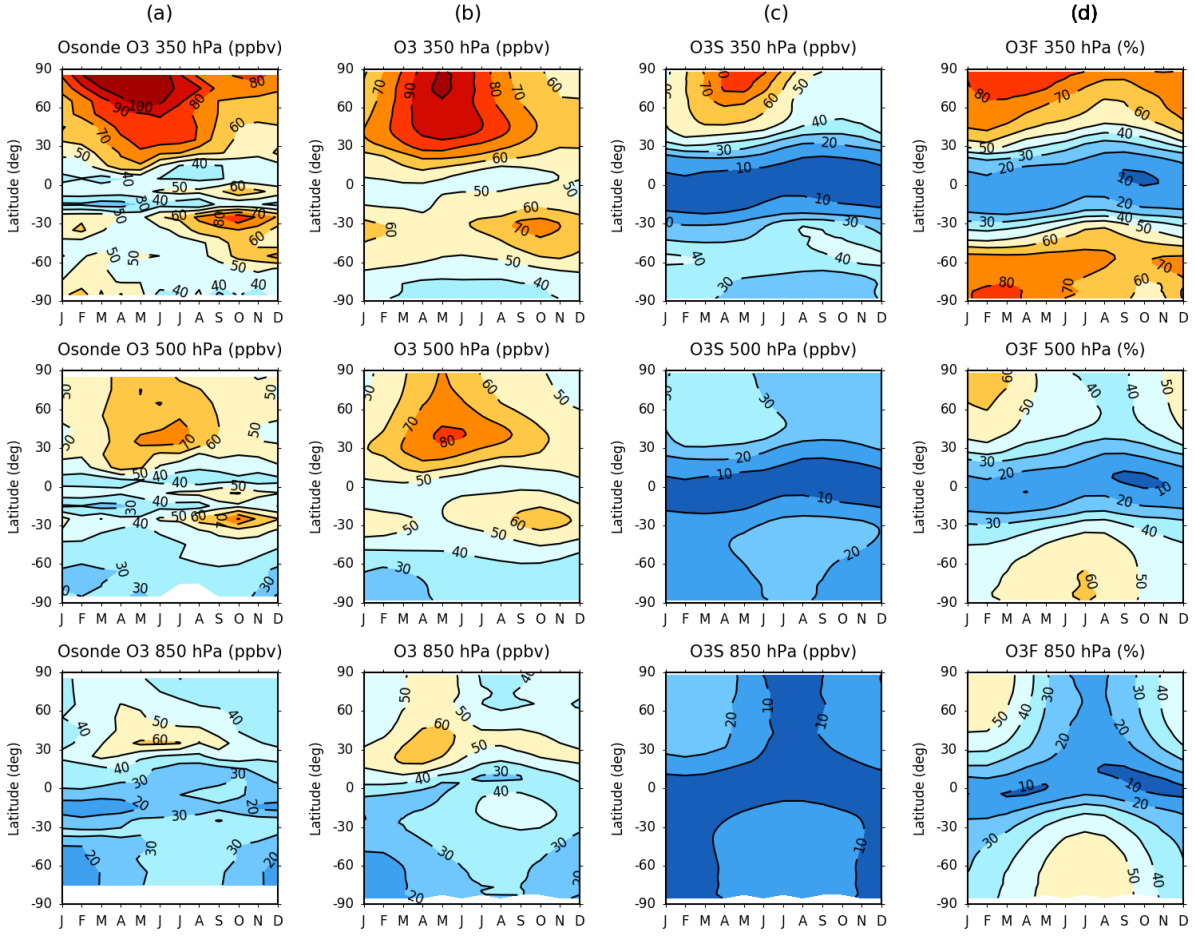

Figure 7 – Zonal-mean monthly mean evolution of O_3 VMR concentration (ppbv) derived from (a) ozonesondes and (b) EMAC O_3 model tracer. The evolution of the (c) EMAC stratospheric O_3S tracer and (d) O_3F stratospheric fraction (%) are additionally included over the period 1980-2010 for 350 hPa (top row), 500 hPa (middle row) and 850 hPa (bottom row).

of O_3 and O_3S are evident in the contemporary CCM simulations, as well as higher stratospheric fraction (O_3F) values.

The EMAC O_3S evolution corresponds closely to the O_3 evolution at 350 hPa, reflecting the large contribution of the stratosphere in the upper troposphere ozone burden (shown also in the O_3F evolution), but this correspondence falls sharply towards the surface (850 hPa) as noted in section 4.2 from Fig. 6. It is important to note that a pronounced spring maximum in O_3S (> 60 ppbv at 350 hPa) is only evident in the Northern Hemisphere, with a much smaller, short-lived maximum between 30° S and 60° S (~ 40 ppbv at 350 hPa), due to the combined influence of the springtime Antarctic ozone hole and a weaker BDC in the Southern Hemisphere which constrains the seasonality. The ozone hole influence is particularly apparent at 350 hPa in each model O_3F evolution fields (d), where the strong symmetry between each hemisphere is briefly interrupted during SON when the ozone hole readily develops over the Southern Hemisphere high-latitudes. The O_3F evolution shows again the sharp meridional gradient in the stratospheric influence, particularly in the upper troposphere, which separates the tropical zone of convective upwelling from the region of net subsidence in both hemispheres where net STE is downward. The seasonality in extratropical O_3F is greater towards the surface due to the competing influence of precursor emissions. Despite this, Fig 7. (bottom row) shows that the stratosphere still contributes about half (~ 50 %) of the amount of ozone during winter at high latitudes at 850 hPa, implying that the stratosphere has a significant influence on near-surface ozone levels, and in turn air quality. This fraction is slightly higher in the Southern Hemisphere due to the lower abundance of precursors compared with the Northern Hemisphere.

4.4 Summary

In summary of this section, use of the model stratospheric ozone (O_3S) tracers reveals a significant difference in the strength and dominance of the shallow branch of the BDC in each model, which has implications for both the simulated downward flux of ozone from the stratosphere and its influence on the relative contribution of stratospheric ozone to tropospheric ozone. CMAM simulates a faster, shallower BDC as inferred from Fig. 5 (section 4.1) which shows between 50-100 % more ozone in the extratropical UTLS region (equating to as much as a +50 ppbv difference), which contrasts with a negative difference in the tropics of between 0 and 30 % (0 to -20 ppbv difference) relative to EMAC within this region (~ 200-400 hPa). It is inferred from characterisation of the vertical ozone distribution biases in Fig. 4 (section 3) that EMAC more accurately depicts the BDC and its effects on the meridional variation in stratospheric ozone, although it is likely that this model is still too conservative in this aspect compared to reality, given a smaller, but general negative stratospheric ozone bias (up to 10-20 %) in the extratropics with respect to ozonesondes. The same inference is in turn made for STE of ozone; a larger proportion of the downward flux of ozone is modelled over the subtropics in comparison with EMAC which simulates a larger flux in the extratropics (Fig. 6 and Fig. S3) . The difference is particularly large in the Southern Hemisphere subtropics (0°-30° S), with a typically larger fraction of stratospheric ozone ranging from 10-25 % from the lower to upper troposphere in CMAM relative to EMAC during austral winter (JJA). There is indication of a preferential STE pathway over the western Indian Ocean and

neighbouring east Africa which is active during this season as far down as the PBL according to CMAM, although any preferential pathway or STE 'hotspot' in this region is not obvious in EMAC or widely established in the literature. Further work is necessary to understand how realistic the representation of STE is in each model, together with the simulated in situ photochemical production of ozone from precursor emissions. Reference to the earlier work of Lamarque et al. (1999) shows that the contemporary CCM simulations analysed in this study more closely match the ozonesonde-derived climatology, which is remarkably consistent in both this study and that produced by Lamarque et al. (1999, Fig. 1, p. 26367), compared to the chemistry transport model (CTM) selected in their study which underestimated tropospheric ozone concentrations by as much as 20-50 %. Both the stratospheric ozone and derived stratospheric fraction fields in their study show very conservative numbers relative to that calculated in this study for both EMAC and CMAM, indicating that the stratosphere has a much larger influence than previously thought, although differences in the stratospheric tracer definitions might explain some of this difference. Both contemporary simulations suggest a significant stratospheric influence on even lower tropospheric ozone, of over 50 % during wintertime in the extratropics which is significantly higher than the 10-20 % estimated from the CTM in Lamarque et al. (1999).

5. Recent Changes in Tropospheric O_3 and O_3S

Seasonal changes in the global mean tropospheric ozone distribution between 1980-89 and 2001-10 are next quantified using the CCM simulations, together with changes in attribution from the stratosphere. The changes in the model ozone (O_3) concentration (VMR) tracers between these two periods are shown globally in Fig. 8 (Fig. S5) at 350 hPa, 500 hPa and the surface model level, as well as throughout the troposphere for three different latitudinal cross sections (30°W, 30°E and 90°E) in Fig. 9 (Fig. S6) for MAM/SON (DJF/JJA). The respective changes in the model stratospheric ozone (O_3S) concentration (VMR) tracers are then shown globally in Fig. 10 (Fig. S7) for each level and as a function of pressure for each latitudinal cross section in Fig. 11 (Fig. S8). Zonal-mean changes in each model tracer are additionally summarised in Table S3 (O_3) and Table S4 (O_3S) for 30° latitude bands.

5.1 O_3 Change (1980-89 to 2001-10)

It is evident in Fig. 8 that both models simulate an overall increase in ozone, which is typically largest (in absolute terms) and most robust (statistically significant) in the upper troposphere (350 hPa) and across the Northern Hemisphere in both seasons. The increase here in both MAM and SON is on the order of some 4-6 ppbv (5-10 %), although in excess of 6 ppbv across some regions during MAM and in CMAM especially, with only a slight lesser overall increase evident at 500 hPa (mid-troposphere). Greater spatial variability is evident at 350 hPa (at least in MAM) due to enhanced sensitivity to changes in the tropopause altitude at this level. This can be inferred from Fig. 9 in the Northern Hemisphere for the 30°W latitudinal cross section in particular, where relatively large apparent model disagreement at 350 hPa can be attributed to a slight downward

Atmos. Chem. Phys. Discuss., https://doi.org/10.5194/acp-2018-1026
Manuscript under review for journal Atmos. Chem. Phys.
Discussion started: 30 October 2018

Atmospheric Chemistry and Physics Discussions

shift in CMAM relative to EMAC; consistent with that found in sections 3 and 4. Relative to CMAM, the largest increases in EMAC are shifted equatorward (~ 10-40°N) and are collocated more closely with the region influenced by the subtropical jet stream (e.g. Manney and Hegglin, 2018), particularly in spring (MAM). In contrast, the largest changes in CMAM are generally poleward of 30°N, particularly at the 350 hPa level. The spatial distribution in the changes is also less zonally consistent than

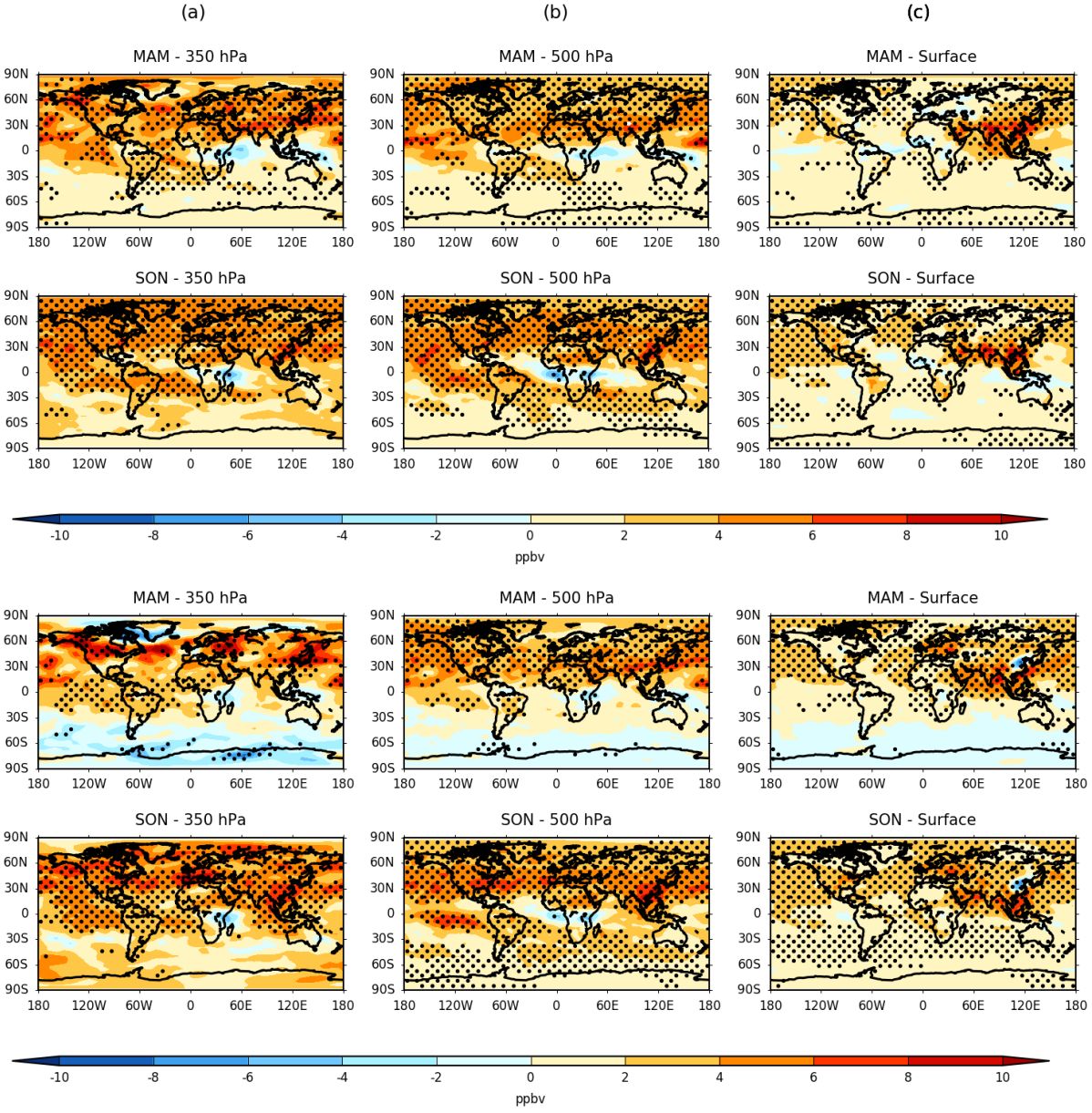

Figure 8 – Seasonal change in EMAC (top) and CMAM (bottom) ozone (O_3) VMR concentration (ppbv) between 1980-89 and 2001-10 for MAM and SON at (a) 350 hPa, (b) 500 hPa and (c) the surface model level. Stippling denotes regions of statistical significance according to a paired two-sided t-test ($p < 0.05$).

Atmos. Chem. Phys. Discuss., https://doi.org/10.5194/acp-2018-1026
Manuscript under review for journal Atmos. Chem. Phys.
Discussion started: 30 October 2018

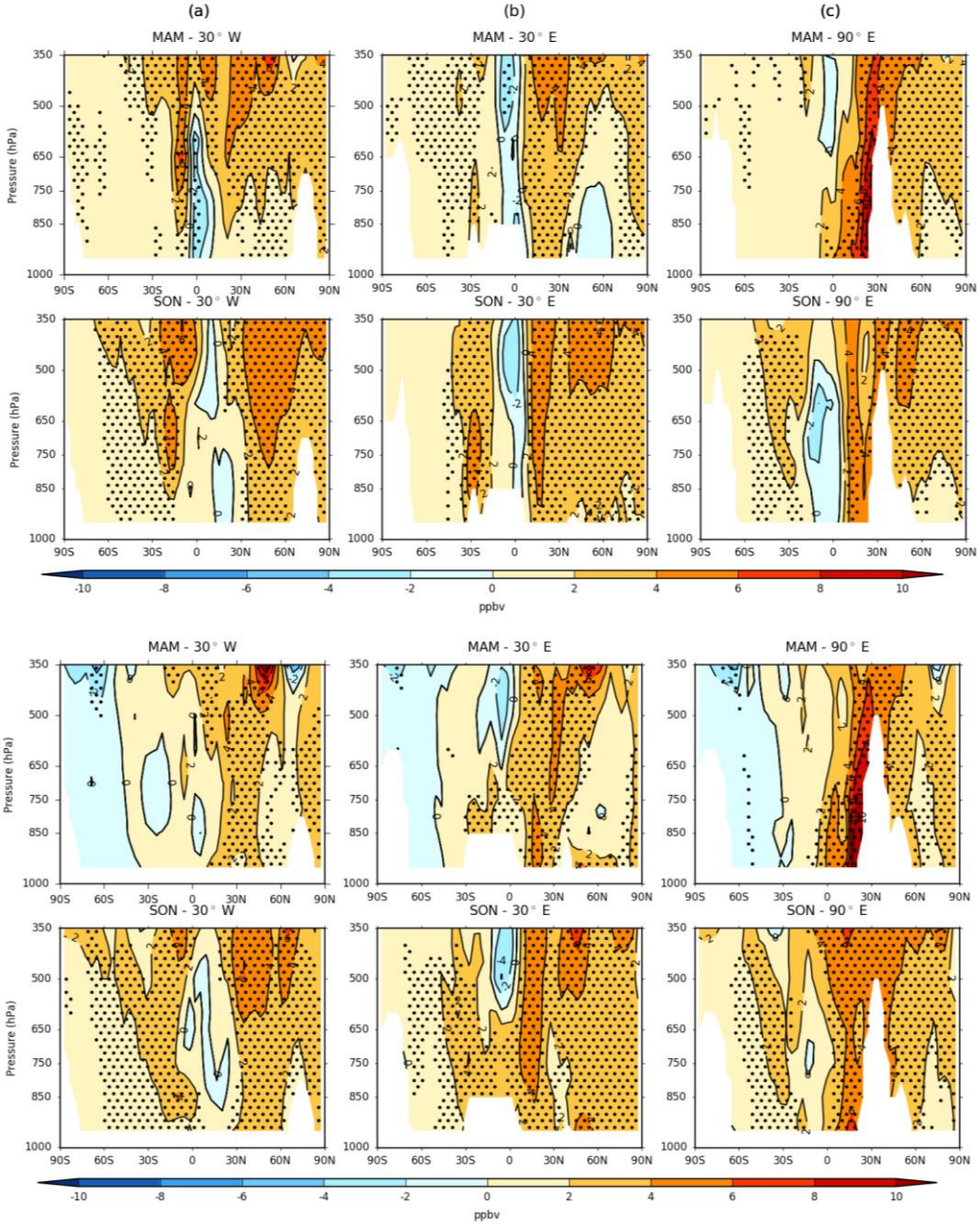

Figure 9 – Longitudinal cross-sections of the seasonal change in the vertical distribution of ozone (O_3) VMR (ppbv) from EMAC (top) and CMAM (bottom) between 1980-89 and 2001-10 for MAM and SON at (a) 30° W, (b) 30° E and (c) 90° E. Stippling denotes regions of statistical significance according to a paired two-sided t-test ($p < 0.05$).

for EMAC, and this could reflect a greater influence in the eddy-driven (polar) jet stream in modulating such spatial variability.

Northern Hemisphere surface changes show greater regional variability due to the strong dependence of the surface environment as both a source of emission precursors and as a sink of ozone. In both seasons, the largest statistically significant increases can be found over south east Asia (exceeding 6 ppbv locally), except for a small region of decrease over north-east China apparent only in CMAM. The 90°E latitudinal cross section in Fig. 9 intersects this region, showing the largest increase close to the southern flank on the Himalayas in each model during both MAM (+6-10 ppbv) and SON (+4-6 ppbv), extending from the surface upwards towards the UTLS (350 hPa). A significant increase is also evident widely over oceanic regions, particularly in CMAM and in SON where values exceed 2 ppbv. This could be attributable to a number of factors, including increases in emissions from international shipping, long range transport from upstream precursor emission sources as well as enhanced subsidence in mid-latitudes due to the influence of subtropical high pressure systems (e.g. the Azores High and the North Pacific High) which may have expanded and intensified in recent decades (Li et al., 2011; 2012). Long range transport has a clear dominant influence over the Pacific sector, as expected due to the rapid advection from this region. Given recent emission controls in North America, and therefore smaller changes in surface ozone, this factor would be less influential over the Atlantic. Across Europe, there is a large discrepancy in the long term changes between the two models, with negligible change in EMAC (or even slightly negative in MAM) but considerable increase (~ 2-6 ppbv) in CMAM in both seasons. Fig. 10 later shows that this difference is at least partly related to the simulated downward flux of stratospheric ozone in each model during spring (MAM) but not in autumn (SON), with the remaining difference likely related to the chemistry schemes in each model. It is however noted from Jöckel et al. (2016) that the timing of road traffic emissions is offset in this EMAC simulation, leading to a slight underestimation of tropospheric partial column ozone (up to ~ 1.5 DU in Northern Hemisphere mid-latitudes during boreal summer between 2000 and 2013), but any impact on calculated ozone changes or trends has not yet been quantified.

Smaller, largely statistically insignificant changes are typically found over the tropics and across parts of the Southern Hemisphere in both models, but particularly in CMAM and during autumn (MAM) when changes are near-zero or even negative. Between 0°N and 30°S, a continuous region of statistically significant increase in ozone (~ 2-6 ppbv) is however apparent along a north-west to south-east axis over the Pacific, South America and South Atlantic at both 350 and 500 hPa; largest and most coherent in EMAC and during SON, particularly over the Pacific Ocean. The geographical orientation of this feature is consistent with the climatological positioning of the Southern Hemisphere subtropical jet stream. Over Africa, a relatively small region of decrease (along or slightly south of the equator) is present in both seasons, in both models at 350 and 500 hPa. The largest decreases are evident in SON, where locally ozone has decreased at a rate of 4-6 ppbv. This feature is not always statistically significant, likely due to its small-scale and subsequent enhanced sensitivity to interannual variability. The latitudinal cross section through 30°E in Fig. 9 shows this feature to be most pronounced in the mid- to upper- troposphere in each model (even absent in CMAM in the lower troposphere). The bimodal structure of the changes in ozone (with an increase to the south of this region) is again consistent with a poleward shift in the subtropical upper tropospheric jets as found in Manney and Hegglin (2018) and the location of STE. During autumn (MAM), CMAM shows a decrease over much of the

Atmos. Chem. Phys. Discuss., https://doi.org/10.5194/acp-2018-1026
Manuscript under review for journal Atmos. Chem. Phys.
Discussion started: 30 October 2018

Atmospheric Chemistry and Physics Discussions

extratropics (statistically significant in places at 350 hPa) which could be related to the effects of stratospheric ozone depletion, and the influence this may have on STE of ozone. Ozone depletion principally occurs however during spring (SON) so any apparent delayed impact on tropospheric ozone would need to be investigated further.

5.2 O_3S Change (1980-89 to 2001-10)

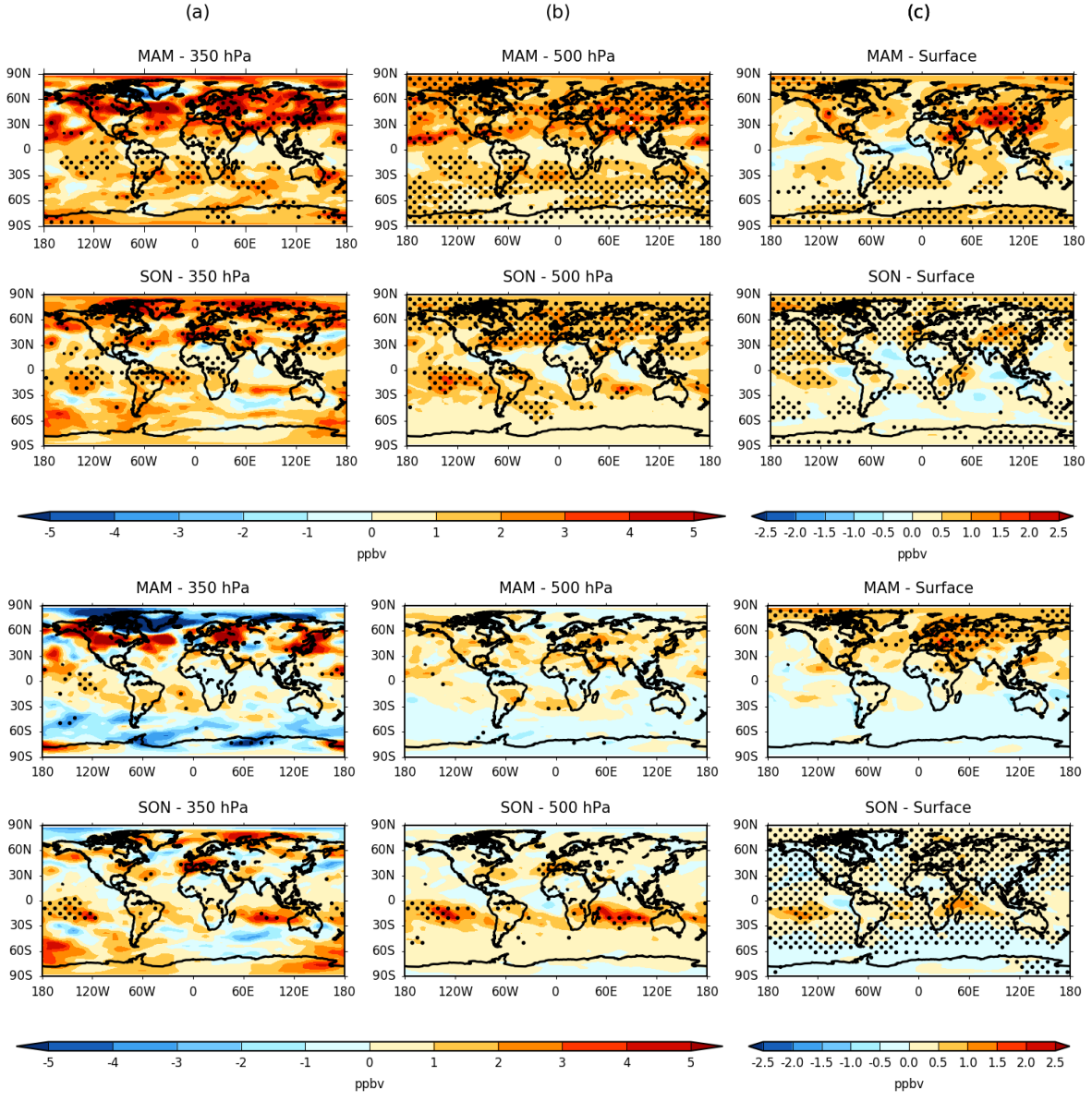

Figure 10 – Seasonal change in EMAC (top) and CMAM (bottom) stratospheric ozone (O_3S) VMR concentration (ppbv) between 1980-89 and 2001-10 for MAM and SON at (a) 350 hPa, (b) 500 hPa and (c) the surface model level. Stippling denotes regions of statistical significance according to a paired two-sided t-test ($p < 0.05$). Note the scale difference between (a-b) and (c).

Atmos. Chem. Phys. Discuss., https://doi.org/10.5194/acp-2018-1026
Manuscript under review for journal Atmos. Chem. Phys.
Discussion started: 30 October 2018

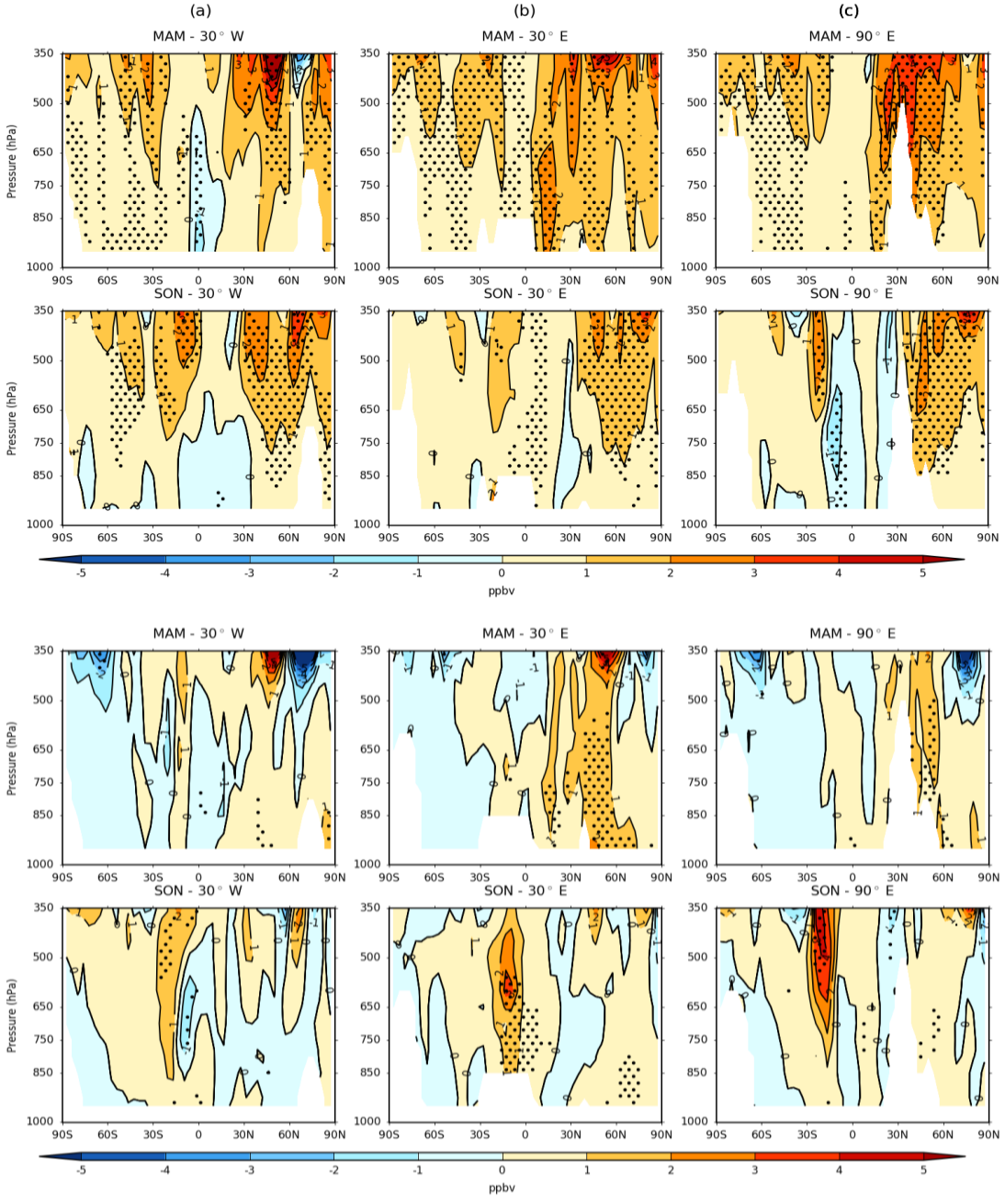

Figure 11 – Longitudinal cross-sections of the seasonal change in the vertical distribution of stratospheric ozone (O_3S) VMR (ppbv) from EMAC (top) and CMAM (bottom) between 1980-89 and 2001-10 for MAM and SON at (a) 30° W, (b) 30° E and (c) 90° E. Stippling denotes regions of statistical significance according to a paired two-sided t-test ($p < 0.05$).

The long term changes in the corresponding stratospheric ozone (O_3S) model tracers shown in Fig. 10 and 11 (Fig. S7 and S8)

for MAM/SON (DJF/JJA) help attribute the long term changes in O_3 described above primarily to either changes in STE or due to changes occurring in the troposphere, such as the photochemical production of ozone from precursors as well as changing tropospheric transport regimes. Similarly to the changes in O_3, both the largest spatial variability and changes in O_3S are evident towards the upper troposphere (350 hPa), particularly in the Northern Hemisphere where an overall increase can again be seen between both periods. The largest increases in O_3S span across the mid-latitudes in the Northern Hemisphere (particularly during MAM), with extensive regions of +3-5 ppbv or greater and +2-4 ppbv in both models during spring (MAM) and autumn (SON) respectively, although statistical significance is often lacking in CMAM especially; indicating the high level of interannual variability in upper tropospheric dynamics. This can again be inferred from the spatial change patterns in the upper troposphere in the latitudinal cross sections in Fig. 11 (Fig. S8) but most notably along the 30°W meridian, where subtle shifts in the height of tropopause and associated sharp gradient in ozone concentrations can at least partly explain the large discrepancies between the models in both the sign and magnitude of changes for any given region at the 350 hPa pressure level. Both models are however consistent in showing statistically significant increases in the regions of the subtropical jet, but particularly in EMAC, which is also evident in the mid-troposphere (500 hPa). In contrast, the models differ significantly at high latitudes, especially in MAM when CMAM shows a large decrease (>-5 ppbv) over parts of NE Canada, Southern Greenland and Northern Siberia. Although EMAC shows a few localised regions of slight decrease, which are spatially collocated with CMAM, the model is dominated by an increase in O_3S at these latitudes. Together with intermodel discrepancies in tropopause height, the spatial distribution in changes during MAM (most notably in CMAM) could reflect an equatorward shift in the mean position of the eddy-driven polar jet stream over time, and the subsequent area of preferential downward STE, which has been identified through trend analyses using reanalysis datasets (Manney and Hegglin, 2018). Conversely, changes at 500 hPa are much more spatially uniform, although large differences remain between the two models. Surface changes in O_3S on the other hand are generally modest, with the large role of precursor emissions in contributing to the increase in O_3 (Fig. 8) obvious across many regions, most notably over SE Asia, when comparing such changes with the calculated changes in the model O_3S tracers. Nonetheless, some regions (e.g. western North America and Eurasia) show an increase of 1-2 ppbv in MAM (locally significant), which represents a large fraction of the corresponding increase in O_3 (or even an offset of a slight negative change over parts of Europe in EMAC) as previously shown in Fig. 8. The main difference between the two models is the larger relative increase in O_3S in EMAC across much of the Middle East and central southern Asia, and conversely across much of Europe and western Eurasia in CMAM. The former difference is additionally highlighted in the 90°E transect (Fig. 11) which intersects the Himalayan region, although both models show a statistically significant increase (> 1 ppbv) in spring (MAM) along the northward flank of the mountain range which represents a minimum contribution of ~ 25-30 % to the surface ozone change of 2-4 ppbv (Fig. 9) Regional discrepancies are smaller in SON with a general, albeit smaller, increase in O_3S (~ +0-1 ppbv) apparent, which is most pronounced in EMAC. Interestingly, changes during this season are widely statistically significant in direct contrast with MAM across most regions, although the climatological influential of the stratosphere is least during this season.

Changes in O_3S across the tropics at both 350 and 500 hPa are generally small, consistent and of similar magnitude between each model, during both MAM and SON, reflecting the absence of influence from the stratosphere (typical tropical tropopause altitude of ~ 100 hPa in the tropics) and a general upwelling regime. In the Southern Hemisphere subtropics however, both models show hemispheric-wide, sometimes statistically increases in O_3S on the order of ~ +1-4 ppbv centred between 10-30°S, except in CMAM during MAM when any increase is confined over South America and adjacent oceanic regions. Such zonal structure in the spatial trend patterns is strongly supportive of influence from the subtropical jet stream, with the largest changes offset slightly equatorward of the climatological mean position in both seasons as identified in the literature (Langford, 1999; Manney and Hegglin, 2018). Indeed, preferential transport from the stratosphere to the troposphere has a known tendency to occur on the equatorward side of the jet (Lamarque and Hess, 2003). The calculated changes in the O_3S tracer confirms that the O_3 changes (Fig. 8) are primarily driven (> 50 %) by an enhanced influence from the stratosphere, with the increase largest in CMAM during austral spring (SON) in likely association with an increased lower branch in the BDC in this model, which is more pronounced in the Southern Hemisphere (Hegglin et al., 2014; Haenel et al., 2015). Poleward of 30°S, changes are weak and generally insignificant at 500 hPa, with CMAM exhibiting an overall slight decrease during MAM and also in SON over Antarctica, whilst EMAC displays a slight increase generally (only exceeding 1 ppbv on a local basis), most pronounced in MAM where changes are significant in places. The spatial change patterns are broadly similar at 350 hPa, although spatial variability is considerably larger and complex patterns emerge, with particularly large discrepancies during MAM between each model. The differential spatial change patterns in each model at this height could be attributable to a range of factors such as the simulation of stratospheric ozone depletion, changes in the BDC between the two time periods, as well as differences in tropopause altitude in each model. Surface changes in O_3S across the Southern Hemisphere are small (and insignificant in places), although two localised regions of statistically significant increase (locally > 1 ppbv in CMAM) emerge in SON in the tropics; in the central South Pacific and over part of the western Indian Ocean and eastern Africa. The latter region is captured in the 30°E latitudinal cross section (Fig. 11) in CMAM especially, with a clear downward pathway in evidence coupling changes in O_3S from the tropopause to the surface. Both regions are collocated spatially with the area of largest increase in O_3S at both 350 and 500 hPa in the Southern Hemisphere, indicating that the influence of enhanced STE of ozone during SON between 1980-89 and 2001-10 is able to penetrate deep into the PBL in these regions, explaining most of the increase in the model O_3 tracers locally here.

5.3 Summary

To summarise, changes in seasonal mean tropospheric ozone are generally positive between 1980-89 and 2001-10 in both models, with a maximum increase of approximately 4-6 (2-6) ppbv (~ 5-10 %) over the Northern Hemisphere (Southern Hemisphere subtropics) during springtime in both the middle (500 hPa) and upper troposphere (350 hPa). A significant stratospheric contribution to such increase is found here of up to 3-5 (1-4) ppbv during this season (~ 50-80 %), although significant intermodel disagreement exists in the magnitude and sometimes the sign of the attributable change in ozone due to

the stratosphere for any given region or season. This is particularly the case in the extratropics, where different responses to transport likely arise in each model resulting from nudging to specified dynamics as captured in ERA-Interim. Both the ozone (O_3) and stratospheric ozone (O_3S) tracers exhibit a preferential increase in the subtropics (extratropics) in EMAC (CMAM) which may reflect the relative importance of the subtropical (polar) jet streams respectively. This difference is however larger in the former case, which implies that the higher amounts of simulated ozone from precursor emissions in EMAC, particularly in the Northern Hemisphere subtropics, propagates upward from the surface and longitudinally due to influence of these two jet streams, contributing to this difference. In the tropics and Southern Hemisphere extratropics on the other hand, estimated changes are typically small and insignificant, with some indication of a decrease over high-latitudes in CMAM. This is likely attributable to the influence of stratospheric ozone depletion but this requires further investigation given the lack of model agreement and largest decrease in autumn (MAM), which is not consistent with the timing of the springtime stratospheric ozone hole. Although surface ozone changes are dominated by regional changes in precursor emissions between the two periods – the largest, statistically significant increases (> 6 ppbv) over south-east Asia – the changing influence from the stratosphere is also shown to be highly significant. Indeed, the global area of statistical significance in the calculated O_3S changes typically increases from the upper troposphere (350 hPa) to the surface. Increases in surface ozone driven by the stratosphere are estimated to be up to 1-2 ppbv between the two periods in the Northern Hemisphere, although this is highly variable both regionally and seasonally and between each model. In relative terms, the stratosphere can be seen to typically explain ~ 25-30 % of the surface change over some regions such as the Himalayas, although locally it may represent the dominant driver (> 50 %) where changes in emission precursors are negligible or even declining due to the enforcement of air quality regulations over regions such as Western Europe and Eastern North America.

6. Conclusions

Seasonal variability, stratospheric influence and recent changes in tropospheric ozone are evaluated in this study using two state-of-the-art CCMs, which have the added provision of tagged stratospheric ozone tracer simulations. This study finds evidence that both CCMs are broadly consistent and agree with satellite (OMI) observations and limited in situ (ozonesonde) profile measurements over the 2005-2010 common baseline period, in simulating both the geographical variability and seasonality in tropospheric subcolumn (1000-450 hPa) ozone. Inherent, systematic biases (with a strong seasonal dependence) are however shown to exist in each model. EMAC is characterised by an overall positive bias with respect to OMI, largest in Northern Hemisphere low latitudes during springtime (~ +2-8 DU or +10-30 %). In contrast, CMAM shows no obvious overall bias (~ -4 to + 4 DU or -20 to +20 %) but with significant regional, latitudinal and seasonal variability in both the sign and magnitude of the bias relative to OMI. In CMAM, the seasonal evolution of the biases between OMI and with respect to ozonesondes for three different extratropical regions show larger consistency prior to the application of the satellite (OMI) AKs, which is contrary to that expected through accounting for the observation geometry of the satellite. Whilst the application of AKs serves to mitigate slightly the positive tropospheric bias in mid-latitudes in EMAC, the negative bias in CMAM is

converted to a positive bias generally in mid- to high-latitudes. Comparisons with sondes indicates that the low tropospheric bias in CMAM, likely related to the simplicity of the model chemistry scheme, is offset due to an inherent high ozone bias in the lowermost stratosphere (as high as 40-60 %). This leads to excessive downward smearing of ozone into the troposphere as a result of applying satellite (OMI) AKs, necessary to compare both model simulation and OMI satellite measurements equivalently. The high bias in mid-latitudes in EMAC is likely explained by a combination of the relatively complex tropospheric chemistry scheme and possible overestimation of emissions. Given the largest tropospheric biases are equatorward of the region greater influenced by vertical smearing from the lowermost stratosphere, the two influences are more independent in this model. The relative importance of these drivers is regionally and seasonally dependent but serves to yield an overall lower bias in CMAM compared with EMAC. The influence of applying AKs is typically to increase the subcolumn amount of tropospheric ozone (1000-450 hPa) in the extratropics by ~ 1-5 DU or ~ 2-8 DU in EMAC and CMAM respectively, depending on season, whereas a slight decrease (~ 0-1 DU) is induced in the tropics in all seasons. An exception to this is over the Southern Hemisphere high latitudes, where the increase is significantly lower due to influence of the ozone hole, particularly in austral spring (SON) when any increase is negligible (0-1 DU). It is important to note that like models, satellite retrieval platforms such as OMI have their own limitations, such as the susceptibility to instrument noise. It is suspected that this limitation is the cause of the large discrepancy in the seasonal composites of RSD, as a metric for the interannual variability, between OMI and the models; the latter of which is in closer agreement with that derived from ozonesondes. A general consensus in the interannual variability in tropical tropospheric ozone is however found, with RSD values of over 10 % in some regions and seasons, consistent with the known influence of a number of different teleconnection drivers such as ENSO and the QBO. Inconsistencies in a number of the model-OMI and model-ozonesonde differences are also suspected to undermine the issue of resolution (in the case of models) and signal-to-noise ratio (in the case of OMI) in adequately resolving mesoscale features, such as local scale pollution plumes or stratospheric intrusion (tropopause folding) events, although this would be an area warranting further investigation.

Taking this information into account, the relatively long temporal span of the specified dynamics CCM simulations was utilised to investigate the climatological stratospheric influence on tropospheric ozone and calculate estimated recent changes between 1980-89 and 2001-10. A clear difference in the strength and dominance of the shallow branch of the BDC was found in each model. The characterised biases with respect to ozonesondes indicate that CMAM has a faster, shallower BDC compared to actuality, which can be inferred from the high lower stratospheric ozone bias (~ +20-60 %), whereas EMAC provides a more realistic simulation of the BDC, albeit perhaps too conservative given a general negative ozone bias (up to 10-20 %) in the lower stratosphere. The difference in BDC simulation has implications for the simulated STE flux of ozone; with preferential downward transport in the subtropics in CMAM compared with the mid-latitudes in EMAC, particularly in the Southern Hemisphere subtropics and during springtime when the difference is as much as 10-25 % from the lower to upper troposphere. Compared to the model results of Lamarque et al. (1999), the CCM simulations examined here are in much closer agreement with ozonesonde measurements (no larger than 20 %) as evidenced on a zonally averaged, monthly basis in Fig. 7 (Fig. S4),

in contrast to a systematic underestimation of tropospheric ozone concentrations by as much as 20-50 % in the CTM analysed in their study. Despite a significant fall in the correspondence between the seasonal evolution of the simulated ozone and stratospheric ozone component in the CCMs from the upper to lower troposphere, the results show a significant stratospheric influence on even lower tropospheric ozone – greater than 50 % in the wintertime extratropics, which contrasts with a modest 10-20 % estimated from the CTM in Lamarque et al. (1999).

Both models show an overall, statistically significant increase in ozone between 1980-89 and 2001-10, on the order of 4-6 (2-6) ppbv (~ 5-10 %) across the Northern Hemisphere (Southern Hemisphere subtropics) in the middle to upper troposphere, with a preferential increase over the subtropics in EMAC compared to the extratropics in CMAM (most pronounced in spring). The stratosphere is found to provide a substantial contribution ranging between 1-3 ppbv (~ 20-50 %) in the mid-troposphere (500 hPa) and over 5 ppbv (~ 50-80 %) in the upper troposphere (350 hPa) across the Northern Hemisphere mid-latitudes, with a typical increase of 1-4 ppbv (~ 50-80 %) over the Southern Hemisphere subtropics at both pressure levels. Significant model disagreement however exists, particularly in the extratropical upper troposphere, likely due to high sensitivity to the tropopause and variability in upper level dynamics which may be affected by the nudging applied to the models. Estimated changes in ozone and the stratospheric contribution on the other hand are generally small and insignificant in both equatorial and Southern Hemisphere extratropical regions. The spatial pattern of changes in surface ozone in contrast show a very different character, with the largest statistically significant increases over much of south-east Asia (> 6 ppbv) and a general increase of up to 2 ppbv or higher quite widely over Northern Hemisphere oceanic regions, but only very small, non-significant changes across the Southern Hemisphere. The influence from the stratosphere at the surface is seen to have a strong regional and seasonal dependence, but is estimated to be as much as 1-2 ppbv during spring, which was estimated to be as large as ~ 25-30 % along the northern flank of the Himalayan mountain range and greater than 50 % over a localised, relatively unpolluted region of Eastern Africa and the Western Indian Ocean. The situation is complicated in some regions however where near-zero or slight negative changes in ozone concentration are apparent in places such as Western Europe and Eastern North America, corresponding to an observed hiatus or slight fall in precursor emissions.

This study highlights some of the shortcomings of both the EMAC and CMAM CCMs as part of the IGAC/SPARC CCMI activity, as validated with respect to satellite observations from OMI and in situ ozonesonde measurements, in simulating tropospheric ozone. In particular, the importance of a well-resolved stratosphere is clear in attaining a high level of model-measurement agreement and in terms of adequately representing stratospheric influence. For comparisons with satellite observational datasets, a well-resolved stratosphere is of paramount importance for the application of AKs which smooth the vertical distribution of model simulated ozone, by smearing information down from the stratosphere to the troposphere. Using this derived knowledge, this study confirms the strong influence of the stratosphere in modulating tropospheric ozone and provides an indication that such influence may in fact be much larger than previously thought. Furthermore, recent changes in tropospheric ozone are shown to have a large attribution from the stratosphere, which is quantified here in relation to influence

of changing precursor emissions. A general increase in the amount of stratospheric ozone in the troposphere between 1980-89 and 2001-10 according to both CCMs, which is statistically significant in some regions of the world, would be expected from observed long term changes in the shallow branch of the BDC (Hegglin et al., 2014), in which transit times have been found to exhibit a steady decrease (Bönisch et al., 2011). Indeed, a strengthening of the BDC is postulated to be the main mechanism for an expected increase in STE under future climate change scenarios (Hegglin and Shepherd, 2009; Butchart et al., 2010), which further highlights the need for an improved understanding of the relationship between STE and tropospheric ozone and accurate quantitative estimates. These findings thus have important implications for the enforcement of both current and future air quality regulations, as well as in constraining estimates of tropospheric ozone radiative forcing.

Data Availability

All CCM simulations analysed here are publicly available from CEDA/BADC via the CCMI data archive (www.ceda.ac.uk). L3 data from OMI using the RAL profiling scheme can be provided on request by contacting barry.latter@stfc.ac.uk. Ozonesonde profile data is publicly accessible from the WOUDC database (www.woudc.org).

Author Contribution

RSW (the lead author) designed the research study, undertook the analyses and prepared the manuscript under the close supervision of MIH, with some additional supervisory support from BK. BL produced and provided access to OMI-RAL L3 data, with both BK and BL able to offer technical support on the satellite (OMI) dataset. Similarly, PJ and DP provided technical support in relation to the EMAC and CMAM CCM simulation datasets respectively. All co-authors provided comments and suggestions helping RSW to greatly improve the quality of the manuscript.

Competing Interests

The authors declare that they have no conflict of interest.

Acknowledgments

RSW would like to personally thank the Natural Environmental Research Council (NERC) for funding the research and each co-author in providing their support and expertise in shaping the research study and the design of the manuscript. We acknowledge the modelling groups for making their simulations available for this analysis, the joint WCRP SPARC/IGAC Chemistry-Climate Model Initiative (CCMI) for organizing and coordinating the model data analysis activity, and the British Atmospheric Data Centre (BADC) for collecting and archiving the CCMI model output.

References

Allen, D. J. and Pickering, K. E.: Evaluation of lightning flash rate parameterizations for use in a global chemical transport model. J. Geophys. Res. Atmos., 107(D23), 4711, doi:10.1029/2002JD002066, 2002.

Akritidis, D., Pozzer, A., Zanis, P., Tyrlis, E., Skerlak, B., Sprenger, M., & Lelieveld, J.: On the role of tropopause folds in summertime tropospheric ozone over the eastern mediterranean and the middle east, Atmos. Chem. Phys., 16(21), 14025-14039. doi:10.5194/acp-16-14025-2016, 2016.

Bethan, S., Vaughan, G. and Reid, S. J.: A comparison of ozone and thermal tropopause heights and the impact of tropopause definition on quantifying the ozone content of the troposphere, Q.J.R. Meteorol. Soc., 122: 929-944. doi:10.1002/qj.49712253207, 1996.

B. Bolin: On the Influence of the Earth's Orography on the General Character of the Westerlies, Tellus, 2:3, 184-195, doi:10.3402/tellusa.v2i3.8547, 1950.

Bönisch, H., Engel, A., Birner, T., Hoor, P., Tarasick, D. W., & Ray, E. A.: On the structural changes in the brewer-dobson circulation after 2000, Atmos. Chem. Phys., 11(8), 3937. Retrieved from https://search.proquest.com/docview/867784704?accountid=13460, 2011.

Brinkop, S., Dameris, M., Jöckel, P., Garny, H., Lossow, S. and Stiller, G.: The millennium water vapour drop in chemistry–climate model simulations, Atmos. Chem. Phys., 16(13), 8125-8140., doi:10.5194/acp-16-8125-2016, 2016.

Butchart, N., I. Cionni, V. Eyring, T.G. Shepherd, D.W. Waugh, H. Akiyoshi, J. Austin, C. Brühl, M.P. Chipperfield, E. Cordero, M. Dameris, R. Deckert, S. Dhomse, S.M. Frith, R.R. Garcia, A. Gettelman, M.A. Giorgetta, D.E. Kinnison, F. Li, E. Mancini, C. McLandress, S. Pawson, G. Pitari, D.A. Plummer, E. Rozanov, F. Sassi, J.F. Scinocca, K. Shibata, B. Steil, and W. Tian: Chemistry–Climate Model Simulations of Twenty-First Century Stratospheric Climate and Circulation Changes. J. Climate, **23**, 5349–5374, doi:10.1175/2010JCLI3404.1, 2010.

Butchart, N.: The Brewer-Dobson circulation, Rev. Geophys., 52, 157-184, doi:10.1002/2013RG000448, 2014.

Charney, J. G. and Eliassen, A.: A Numerical Method for Predicting the Perturbations of the Middle Latitude Westerlies, Tellus, 1:2, 38-54, doi:10.3402/tellusa.v1i2.8500, 1949.

Cooper, O. R., Parrish, D. D., Stohl, A., Trainer, M., Nédélec, P., Thouret, V., Leblanc, T. et al.: Increasing springtime ozone mixing ratios in the free troposphere over western North America, Nature, 463(7279), 344-348, doi:10.1038/nature08708, 2010.

Cooper, O. R., Parrish, D. D., Ziemke, J., Cupeiro, M., Galbally, I. E., Gilge, S. et al.: Global distribution and trends of tropospheric ozone: An observation-based review, Elem. Sci. Anth. 2, p.29, doi:10.12952/journal.elementa.000029, 2014.

Eyring, V., Lamarque, J. F., Hess, P., Arfeuille, F., Bowman, K., Chipperfiel, M. P. and Granier, C.: Overview of IGAC/SPARC Chemistry-Climate Model Initiative (CCMI) community simulations in support of upcoming ozone and climate assessments. SPARC Newsletter, 40(January), 48-66, Retrieved From: http://oceanrep.geomar.de/20227/, 2013.

Fiore, A. M., D. J. Jacob, B. D. Field, D. G. Streets, S. D. Fernandes, and C. Jang: Linking ozone pollution and climate change: The case for controlling methane, Geophys. Res. Lett., 29(19), 1919, doi:10.1029/2002GL015601, 2002.

Foret, G., Eremenko, M., Cuesta, J., Sellitto, P., Barré, J., Gaubert, B. et al.: Ozone pollution: What can we see from space? A case study, J. Geophys. Res. Atmos., 119, 8476–8499, doi: 10.1002/2013JD021340, 2014.

Gaudel, A., Cooper, O. R., Ancellet, G., Barret, B., Boynard, A., Burrows, J. P. et al.: Tropospheric Ozone Assessment Report: Present-day distribution and trends of tropospheric ozone relevant to climate and global atmospheric chemistry model evaluation. Elementa, 6: 39. doi:10.1525/elementa.291, 2018.

Greenslade, J. W., Alexander, S. P., Schofield, R., Fisher, J. A. and Klekociuk, A. K.: Stratospheric ozone intrusion events and their impacts on tropospheric ozone in the Southern Hemisphere, Atmos. Chem. Phys., 17(17), 10269-10290, doi:10.5194/acp-17-10269-2017, 2017.

Guenther, A., Hewitt, C. N., Erickson, D., Fall, R., Geron, C., Graedel, T. et al.: A global model of natural volatile organic compound emissions, J. Geophys. Res., 100(D5), 8873–8892, doi: 10.1029/94JD02950, 1995.

Haenel, F. J., Stiller, G. P., Von Clarmann, T., Funke, B., Eckert, E., Glatthor, N. et al.: Reassessment of MIPAS age of air trends and variability, Atmos. Chem. Phys., 15(22), 13161-13176, doi:0.5194/acp-15-13161-2015, 2015.

Hegglin, M. I., Brunner, D., Peter, T., Hoor, P., Fischer, H., Staehelin, J. et al.: Measurements of NO, NO_y, N_2O, and O_3 during SPURT: Implications for transport and chemistry in the lowermost stratosphere, Atmos. Chem. Phys., 6(5), 1331-1350. doi:10.5194/acp-6-1331-2006, 2006.

Hegglin, M. I., Gettelman, A., Hoor, P., Krichevsky, R., Manney, G. L., Pan, L. L. et al.: Multimodel assessment of the upper troposphere and lower stratosphere: Extratropics, J. Geophys. Res. Atmos., 115(D3), doi:10.1029/2009JD013638, 2010.

Hegglin, M. I. and J.-F. Lamarque: The IGAC/SPARC Chemistry-Climate Model Initiative Phase-1 (CCMI-1) model data output, NCAS British Atmospheric Data Centre, 24th September 2018. http://catalogue.ceda.ac.uk/uuid/9cc6b94df0f4469d8066d69b5df879d5, 2015.

Hegglin, M. I., Plummer, D. A., Shepherd, T. G., Scinocca, J. F., Anderson, J., Froidevaux, L. et al.: Vertical structure of stratospheric water vapour trends derived from merged satellite data, Nat. Geosci., 7(10), 768–776, doi:10.1038/NGEO2236, 2014.

Hegglin, M. I. and Shepherd, T. G.: Large climate-induced changes in ultraviolet index and stratosphere-to-troposphere ozone flux, Nat. Geosci., 2(10), 687-691, doi:10.1038/NGEO604, 2009.

Holton, J. R., P. H. Haynes, M. E. McIntyre, A. R. Douglass, R. B. Rood, and L. Pfister: Stratosphere-troposphere exchange, Rev. Geophys., 33(4), 403–439, doi:10.1029/95RG02097, 1995.

Holton, J. R. and Lelieveld, J.: Stratosphere-troposphere exchange and its role in the budget of tropospheric ozone. In Clouds, chemistry and climate (pp. 173-190). Springer, Berlin, Heidelberg, 1996.

Hudman, R. C., Jacob, D. J., Cooper, O. R., Evans, M. J., Heald, C. L., Park, R. J. and Kita, K.: Ozone production in transpacific Asian pollution plumes and implications for ozone air quality in California. J. Geophys. Res. Atmos., 109(D23), doi:10.1029/2004JD004974, 2004.

Jöckel, P., H. Tost, A. Pozzer, C. Brühl, J. Buchholz et al.: The atmospheric chemistry general circulation model ECHAM5/MESSy1: consistent simulation of ozone from the surface to the mesosphere. Atmos. Chem. Phys. Discuss. European Geosciences Union, 6(4), 6957-7050, hal-00302020, 2006.

Jöckel, P., Tost, H., Pozzer, A., Kunze, M., Kirner, O., Brenninkmeijer, C. A. et al.: Earth System Chemistry Integrated Modelling (ESCiMo) with the Modular Earth Submodel System (MESSy, version 2.51), Geosci. Model Dev., 8(10), doi:10.5194/gmd-9-1153-2016, 2016.

Komhyr, W. D., R. A. Barnes, G. B. Brothers, J. A. Lathrop, and D. P. Opperman: Electrochemical concentration cell ozonesonde performance evaluation during STOIC 1989, J. Geophys. Res., 100(D5), 9231–9244, doi: 10.1029/94JD02175, 1995.

Krebsbach, M., Schiller, C., Brunner, D., Günther, G., Hegglin, M. I., Mottaghy, D. et al: Seasonal cycles and variability of O_3 and H_2O in the UT/LMS during SPURT. Atmos. Chem. Phys., 6(1), 109-125, doi:10.5194/acp-6-109-2006, 2006.

Lacis, A. A., Wuebbles, D. J., and Logan, J. A.: Radiative forcing of climate by changes in the vertical distribution of ozone, J. Geophys. Res., 95, 9971–9981, doi:10.1029/JD095iD07p09971, 1990.

Lamarque, J. F., Hess, P. G. and Tie, X. X.: Three-dimensional model study of the influence of stratosphere-troposphere exchange and its distribution on tropospheric chemistry. J. Geophys. Res. Atmos., 104(D21), 26363-26372, doi:10.1029/1999JD900762, 1999.

Lamarque, J. F. and Hess, P. G.: Local Processes. Encyclopedia of Atmospheric Sciences, 4, 262-268, 2003.

Langford, A. O.: Stratosphere-troposphere exchange at the subtropical jet: Contribution to the tropospheric ozone budget at midlatitudes. Geophys. Res. Lett., 26(16), 2449-2452, doi:10.1029/1999GL900556, 1999.

Lee, S., D. M. Shelow, A. M. Thompson, and S. K. Miller: QBO and ENSO variability in temperature and ozone from SHADOZ, 1998–2005, J. Geophys. Res., 115, D18105, doi:10.1029/2009JD013320, 2010.

Lelieveld, J., Hoor, P., Jöckel, P., Pozzer, A., Hadjinicolaou, P., Cammas, J. P. et al.: Severe ozone air pollution in the Persian Gulf region. Atmos. Chem. Phys., 9(4), 1396-1403, doi: 10.5194/acp-9-1393-2009, 2009.

Levelt, P. F., van den Oord, G. H., Dobber, M. R., Malkki, A., Visser, H., de Vries, J et al.: The ozone monitoring instrument, IEEE Trans. Geosci. Remote. Sens., 44(5), 1093-1101, doi:10.1109/TGRS.2006.872333, 2006.

Levelt, P. F., Joiner, J. Tamminen, J., Veefkind, P., Bhartia, P. K., Zweers, D. S. et al.: The Ozone Monitoring Instrument: Overview of twelve years in space, Atmos. Chem. Phys., doi:10.5194/acp-2017-487, 2017.

Li, W., L. Li, R. Fu, Y. Deng, and H. Wang: Changes to the North Atlantic Subtropical High and Its Role in the Intensification of Summer Rainfall Variability in the Southeastern United States, J. Climate, 24, 1499–1506, doi:10.1175/2010JCLI3829.1, 2011.

Li, W., Li, L., Ting, M. and Liu, Y: Intensification of Northern Hemisphere subtropical highs in a warming climate, Nat. Geosci., 5(11), 830-834, doi:10.1038/NGEO1590, 2012.

Lin, M., Fiore, A. M., Cooper, O. R., Horowitz, L. W., Langford, A. O., Levy, H. et al.: Springtime high surface ozone events over the western United States: Quantifying the role of stratospheric intrusions, J. Geophys. Res. Atmos., 117(D21), doi:10.1029/2012JD018151, 2012.

Lin, M., Horowitz, L. W., Oltmans, S. J., Fiore, A. M. and Fan, S.: Tropospheric ozone trends at Mauna Loa Observatory tied to decadal climate variability, Nat. Geosci., 7(2), 136-143, doi: 10.1038/NGEO2066, 2014.

Lin, M., Fiore, A. M., Horowitz, L. W., Langford, A. O., Oltmans, S. J., Tarasick, D. et al.: Climate variability modulates western US ozone air quality in spring via deep stratospheric intrusions, Nat. Commun., 6, 7105, doi:10.1038/ncomms8105, 2015.

Lin, S. and R.B. Rood: Multidimensional Flux-Form Semi-Lagrangian Transport Schemes. Mon. Wea. Rev., 124, 2046–2070, doi:0.1175/1520-0493(1996)124<2046:MFFSLT>2.0.CO;2, 1996.

Liu, X., Bhartia, P. K., Chance, K., Froidevaux, L., Spurr, R. J. D., and Kurosu, T. P.: Validation of Ozone Monitoring Instrument (OMI) ozone profiles and stratospheric ozone columns with Microwave Limb Sounder (MLS) measurements, Atmos. Chem. Phys., 10, 2539-2549, doi:10.5194/acp-10-2539-2010, 2010.

Logan, J. A.: Tropospheric ozone: Seasonal behavior, trends, and anthropogenic influence, J. Geophys. Res., 90(D6), 10463–10482, doi:10.1029/JD090iD06p10463, 1985.

Manney, G. L. and Hegglin, M. I.: Seasonal and Regional Variations of Long-Term Changes in Upper-Tropospheric Jets from Reanalyses, J Clim, 31(1), 423-448, doi:10.1175/JCLI-D-17-0303.1, 2018.

Mauzerall, D. L., Logan, J. A., Jacob, D. J., Anderson, B. E., Blake, D. R., Bradshaw et al.: Photochemistry in biomass burning plumes and implications for tropospheric ozone over the tropical South Atlantic. J. Geophys. Res. Atmos., 103(D7), 8401-8423, doi:10.1029/97JD02612, 1998.

McLandress, C., J.F. Scinocca, T.G. Shepherd, M.C. Reader, and G.L. Manney: Dynamical Control of the Mesosphere by Orographic and Nonorographic Gravity Wave Drag during the Extended Northern Winters of 2006 and 2009. J. Atmos. Sci., 70, 2152–2169, doi:10.1175/JAS-D-12-0297.1, 2013.

Merryfield, W. J., McFarlane, N. and Lazare, M. A generalized hybrid transformation for tracer advection, WGNE Blue Book, WMO, 3, 13-3, 2003.

Mielonen, T., De Haan, J. F., Van Peet, J. C. A., Eremenko, M. and Veefkind, J. P.: Towards the retrieval of tropospheric ozone with the Ozone Monitoring Instrument (OMI). Atmos. Meas. Tech., 8(2), 671-687, doi:10.5194/amt-8-671-2015, 2015.

Miles, G. M., Siddans, R., Kerridge, B. J., Latter, B. G. and Richards, N. A. D.: Tropospheric ozone and ozone profiles retrieved from GOME-2 and their validation, Atmos. Meas. Tech., 8(1), 385-398, doi:10.5194/amt-8-385-2015, 2015.

Morgenstern, O., Hegglin, M. I., Rozanov, E., O'Connor, F. M., Abraham, N. L., Akiyoshi, H. et al.: Review of the global models used within phase 1 of the Chemistry-Climate Model Initiative (CCMI), Geosci. Model Dev., 10(2), 639-671, doi:10.5194/gmd-10-639-2017, 2017.

Myhre, G., D. Shindell, F.-M. Bréon, W. Collins, J. Fuglestvedt, J. Huang, D. Koch, J.-F. Lamarque, D. Lee, B. Mendoza, T. Nakajima, A. Robock, G. Stephens, T. Takemura and H. Zhang: Anthropogenic and Natural Radiative Forcing. In: Climate Change 2013: The Physical Science Basis. Contribution of Working Group I to the Fifth Assessment Report of the Intergovernmental Panel on Climate Change [Stocker, T.F., D. Qin, G.-K. Plattner, M. Tignor, S.K. Allen, J. Boschung, A. Nauels, Y. Xia, V. Bex and P.M. Midgley (eds.)]. Cambridge University Press, Cambridge, United Kingdom and New York, NY, USA, 659–740, doi:10.1017/ CBO9781107415324.018, 2013.

Nassar, R., Logan, J. A., Worden, H. M., Megretskaia, I. A., Bowman, K. W., Osterman, G. B. et al.: Validation of Tropospheric Emission Spectrometer (TES) nadir ozone profiles using ozonesonde measurements, J. Geophys. Res. Atmos., 113(D15), doi:10.1029/2007JD008819, 2008.

Paoletti, E., De Marco, A., Beddows, D. C. S. et al.: Ozone levels in European and USA cities are increasing more than at rural sites, while peak values are decreasing, Environ. Pollut., 192(x): 295–9, doi:10.1016/j.envpol.2014.04.040, 2014.

Parrish, D. D., et al. (2014), Long-term changes in lower tropospheric baseline ozone concentrations: Comparing chemistry-climate models and observations at northern midlatitudes, J. Geophys. Res. Atmos., 119, 5719–5736, doi: 10.1002/2013JD021435, 2014.

Pendlebury, D., Plummer, D., Scinocca, J., Sheese, P., Strong, K., Walker, K. et al.: Comparison of the CMAM30 data set with ACE-FTS and OSIRIS: polar regions. Atmos. Chem. Phys. Discuss., 15(21), 12465-12485, doi:10.5194/acpd-15-11179-2015, 2015.

Prather, M. J., Zhu, X., Tang, Q., Hsu, J., and Neu, J. L.: An atmospheric chemist in search of the tropopause. J. Geophys. Res. Atmos., 116(D4), doi:10.1029/2010JD014939, 2011.

Rayner, N. A., Parker, D. E., Horton, E. B., Folland, C. K., Alexander, L. V., Rowell, D. P. et al.: Global analyses of sea surface temperature, sea ice, and night marine air temperature since the late nineteenth century. J. Geophys. Res. Atmos., 108(D14), doi:10.1029/2002JD002670, 2003.

Richards, N. A. D., Arnold, S. R., Chipperfield, M. P., Miles, G., Rap, A., Siddans, R. et al.: The Mediterranean summertime ozone maximum: global emission sensitivities and radiative impacts. Atmos. Chem. Phys., 13(5), 2331-2345. doi:10.5194/acp-13-2331-2013, 2013.

Roscoe, H. K.: The Brewer–Dobson circulation in the stratosphere and mesosphere – Is there a trend?. Adv. Space. Res., 38(11), 2446-245, doi:10.1016/j.asr.2006.02.078, 2006.

Sander, R., Baumgaertner, A., Gromov, S., Harder, H., Jockel, P., Kerkweg, A., Kubistin, D., Regelin, E., Riede, H., Sandu, A., Taraborrelli, D., Tost, H. and Xie, Z. -Q.: The atmospheric chemistry box model CAABA/MECCA-3.0, Geosci Model Dev.Geoscientific Model Development, 4 (2), 373-380, doi:10.5194/gmd-4-373-2011, 2011

Schenkeveld, V. E., Jaross, G., Marchenko, S., Haffner, D., Kleipool, Q. L., Rozemeijer, N. C. et al. In-flight performance of the Ozone Monitoring Instrument. Atmos. Meas. Tech., 10(5), 1957-1986, doi:10.5194/amt-2016-420, 2017.

Seinfeld, J. H. and Pandis, S. N. Atmospheric chemistry and physics: from air pollution to climate change. John Wiley & Sons, 2016.

Scinocca, J. F., McFarlane, N. A., Lazare, M., Li, J. and Plummer, D.: The CCCma third generation AGCM and its extension into the middle atmosphere, Atmos. Chem. Phys., 8(23), 7055-7074, doi: 10.5194/acp-8-7055-2008, 2008.

Sellitto, P., Bojkov, B. R., Liu, X., Chance, K., and Del Frate, F.: Tropospheric ozone column retrieval at northern mid-latitudes from the Ozone Monitoring Instrument by means of a neural network algorithm, Atmos. Meas. Tech., 4, 2375-2388, doi:10.5194/amt-4-2375-2011, 2011.

Shepherd, T. G.: Transport in the middle atmosphere. J. Meteorol. Soc. Jpn., N Ser. II, 85B, 165-191, doi: 10.2151/jmsj.85B.165, 2007.

Shepherd, T. G., Plummer, D. A., Scinocca, J. F., Hegglin, M. I., Fioletov, V. E., Reader, M. C. et al. Reconciliation of halogen-induced ozone loss with the total-column ozone record. Nat. Geosci., 7(6), 443, doi:10.1038/NGEO2155, 2014.

SPARC: SPARC/IOC/GAW Assessment of Trends in the Vertical Distribution of Ozone. N. Harris, R. Hudson and C. Phillips (eds.), SPARC Report No. 1, WMO Ozone Research and Monitoring Project Report No. 43, available at https://www.sparc-climate.org/publications/sparc-reports/, 1998.

Škerlak, B., Sprenger, M. and Wernli, H.: A global climatology of stratosphere-troposphere exchange using the ERA-Interim data set from 1979 to 2011. Atmos. Chem. Phys., 14(2), doi:10.5194/acp-14-913-2014, 2014.

Staley, D. O.: On the mechanism of mass and radioactivity transport from stratosphere to troposphere, J. Atmos. Sci., 19(6), 450-467, doi:10.1175/1520-0469(1962)019<0450:OTMOMA>2.0.CO;2, 1962.

Stevenson, D. S., Young, P. J., Naik, V., Lamarque, J. F., Shindell, D. T., Voulgarakis, A. and Folberth, G. A.: Tropospheric ozone changes, radiative forcing and attribution to emissions in the Atmospheric Chemistry and Climate Model Intercomparison Project (ACCMIP). Atmos. Chem. Phys., 13(6), 3063-3085, doi:10.5194/acp-13-3063-2013, 2013

Thompson, A. M., Witte, J. C., McPeters, R. D., Oltmans, S. J., Schmidlin, F. J., Logan, J. A. et al.: Southern Hemisphere Additional Ozonesondes (SHADOZ) 1998–2000 tropical ozone climatology 1. Comparison with Total Ozone Mapping Spectrometer (TOMS) and ground-based measurements, J. Geophys. Res., 108, 8238, doi:10.1029/2001JD000967, D2, 2003.

Thompson, A. M., J. C. Witte, H. G. J. Smit, S. J. Oltmans, B. J. Johnson, V. W. J. H. Kirchhoff, and F. J. Schmidlin: Southern Hemisphere Additional Ozonesondes (SHADOZ) 1998–2004 tropical ozone climatology: 3. Instrumentation, station-to-station variability, and evaluation with simulated flight profiles, J. Geophys. Res., 112, D03304, doi:10.1029/2005JD007042, 2007.

Thompson, A. M., Miller, S. K., Tilmes, S., Kollonige, D. W., Witte, J. C., Oltmans, S. J et al.: Southern Hemisphere Additional Ozonesondes (SHADOZ) ozone climatology (2005–2009): Tropospheric and tropical tropopause layer (TTL) profiles with comparisons to OMI-based ozone products, J. Geophys. Res. Atmos., 117(D23), doi: 10.1029/2011JD016911, 2012.

Worden, H. M., Logan, J. A., Worden, J. R., Beer, R., Bowman, K., Clough, S. A. et al.: Comparisons of Tropospheric Emission Spectrometer (TES) ozone profiles to ozonesondes: Methods and initial results, J. Geophys. Res. Atmos., 112(D3), doi:10.1029/2006JD007258, 2007.

Yang, H., G. Chen, Q. Tang, and P. Hess: Quantifying isentropic stratosphere-troposphere exchange of ozone, J. Geophys. Res. Atmos., 121, 3372–3387, doi:10.1002/2015JD024180, 2016.

Young, P. J., Archibald, A. T., Bowman, K. W., Lamarque, J. F., Naik, V., Stevenson, D. S. et al.: Pre-industrial to end 21st century projections of tropospheric ozone from the Atmospheric Chemistry and Climate Model Intercomparison Project (ACCMIP). Atmos. Chem. Phys., 13(4), 2063-2090, doi:10.5194/acp-13-2063-2013, 2013.

Zanis, P., Hadjinicolaou, P., Pozzer, A., Tyrlis, E., Dafka, S., Mihalopoulos, N. et al.: Summertime free-tropospheric ozone pool over the eastern Mediterranean/Middle East. Atmos. Chem. Phys., 14(1), 115-132, doi: 10.5194/acp-14-115-2014, 2014.

Ziemke, J. R., Chandra, S., Labow, G. J., Bhartia, P. K., Froidevaux, L. and Witte, J. C.: A global climatology of tropospheric and stratospheric ozone derived from Aura OMI and MLS measurements. Atmos. Chem. Phys., 11(17), 9237-9251, doi:10.5194/acp-11-9237-2011, 2011.

Ziemke, J. R. and Chandra, S. (2012). Development of a climate record of tropospheric and stratospheric column ozone from satellite remote sensing: evidence of an early recovery of global stratospheric ozone. Atmos. Chem. Phys., 12(13), 5737-5753, doi: 10.5194/acp-12-5737-2012, 2012.